Author/s:
Raavi, PH;Walsh, KJE

Title:
Basinwise Statistical Analysis of Factors Limiting Tropical Storm Formation From an Initial Tropical Circulation

Date:
2020-06-16

Citation:
Raavi, P. H. & Walsh, K. J. E. (2020). Basinwise Statistical Analysis of Factors Limiting Tropical Storm Formation From an Initial Tropical Circulation. Journal of Geophysical Research Atmospheres, 125 (11), https://doi.org/10.1029/2019JD032006.

Persistent Link:
https://hdl.handle.net/11343/275889

Raavi Pavan, Harika (Orcid ID: 0000-0002-6981-1157)
Walsh Kevin, J. E. (Orcid ID: 0000-0002-1860-510X)

Basinwise statistical analysis of factors limiting tropical storm formation from an initial tropical circulation

Pavan Harika Raavi[1, 2,*] and K.J.E Walsh[1, 2]

[1]*School of Earth Sciences, University of Melbourne, Victoria, Australia*

[2]*ARC Centre of Excellence for Climate Extremes, Australia*

For submission to JGR Atmospheres on 22-04-2020

*Corresponding author:

Pavan Harika Raavi

School of Earth Sciences

University of Melbourne, Parkville, Australia

Email: praavi@student.unimelb.edu.au

Key points:

- Prominent environmental and structural differences exist between developing and non-developing circulations.
- The major environmental factors impeding the development of an initial circulation to a Tropical Storm vary from basin to basin.
- Non-developing cases have a weaker protective layer “shear-sheath” around the vortex core at mid-levels, leading to dry-air intrusion.

This is the author manuscript accepted for publication and has undergone full peer review but has not been through the copyediting, typesetting, pagination and proofreading process, which may lead to differences between this version and the Version of Record. Please cite this article as doi: 10.1029/2019JD032006

Abstract

Tropical cyclones (TC) form within a closed circulation region of large-scale disturbances under certain dynamical and thermodynamical conditions. This study investigates differences in the large-scale environmental conditions of a TC 48 hours before the declaration of tropical depression (TDs), comparing those that developed into tropical storms (TSs) with those depressions that did not develop. Here, we apply the Okubo-Weiss Zeta Parameter (OWZP) detection and tracking scheme to ERA-interim reanalysis from 1989-2018, across different ocean basins. The method detects storm-system-scale environmental conditions that favor TC formation. We construct spatial composites of thermodynamical and dynamical quantities for both developing and non-developing depressions, as well as storm-relative streamlines. A statistical index (the Box Difference Index) is used to quantitatively estimate the dominant limiting factors of TS formation from the area-averaged quantities of large-scale variables. The relative contribution of large-scale environmental variables impeding the development of an initial TD to TS differs between ocean basins perhaps due to regional variations in the characteristics of large-scale disturbances and the surrounding environmental conditions. A streamline analysis shows the developing storms have a more pronounced cyclonic core and are protected from external influences by a stronger shear-sheath layer surrounding the core extending from the lower- to mid-troposphere. This study, therefore,

identifies the potential limiting variables and structural differences in an initial circulation that impede TS formation across different ocean basins.

Plain Language Summary:

Tropical cyclones form under certain atmospheric conditions within different large-scale disturbances across various ocean basins. Every year a large number of tropical disturbances form across global ocean basins, but only a few of them develop into tropical cyclones, with a geographical variation in the number of formations. Previous studies on the differences in the environmental conditions of developing versus non-developing tropical disturbances focus on the Atlantic and Pacific Ocean basins due to less observations in other ocean basins. The recent development of the "marsupial pouch" theory of tropical cyclone formation has led to the development of a detection scheme to identify the locations within large-scale disturbances that have the potential for tropical cyclone formation. The detection scheme is tuned to detect the initial tropical depressions in addition to the developed tropical storms (TSs). This scheme helps us to investigate the environmental differences between developing and non-developing tropical depressions in all the ocean basins. The environmental variables inhibiting TS formation differ among ocean basins, with structural differences from the lower

to upper troposphere disrupting sustained convection in non-developing cases. This study, therefore, identifies the potential limiting factors for tropical storm formation across different ocean basins.

1. Introduction:

Tropical cyclones (TCs) are highly destructive extreme events that lead to substantial socio-economic losses, primarily in coastal regions. TCs form under certain favorable thermodynamical and dynamical conditions within closed recirculating regions (Gray, 1968, 1975; Dunkerton et al., 2009). Favorable thermodynamical conditions include sea surface temperatures (SSTs) higher than 26.5^{o}C, a deep layer of a conditionally unstable environment, and moist mid-troposphere (Gray, 1968). Dynamical conditions include weak to moderate vertical wind shear (vector wind difference magnitude between the 850 and 200 hPa), deep organized convection, and locally enhanced values of low-level cyclonic relative vorticity (Gray, 1968, 1975; McBride & Zehr, 1981). Additionally, Gray (1968) suggested that TCs generally do not form within 5 degrees of the equator. Although these conditions are

necessary for TC formation, it is still not clear what are the sufficient conditions, due to multi-scale interactions in the TC formation activity.

TC formation undergoes different stages of development: the first stage involves pre-conditioning of the large-scale environment along with the formation of minimum atmospheric pressure in the lower levels. The second stage involves the formation of a self-sustaining mesoscale vortex and its aggregation, with modest stretching and shearing deformations enabling a near-solid body rotation (Lee et al., 1989; Briegel & Frank, 1997; Ritchie & Holland, 1999; Montgomery et al., 2006b; Dunkerton et al., 2009). Some large-scale disturbances provide suitable conditions such as increasing low-level relative vorticity, convective activity associated with increased updraft strength, and altering the vertical wind shear distribution to conditions favorable for TC formation. These disturbances include: 1) tropical depression type waves also called African Easterly Waves (AEWs) in the North Atlantic (NA) region (Landsea, 1993; Thorncroft & Hodges, 2001); 2) Rossby wave trains induced by a preexisting TC, Pacific easterly waves and synoptic wave trains, or tropical depression type waves in the Western North Pacific (WNP) region (Li & Fu, 2006; Li et al., 2006; Fu et al., 2007; Xu et al., 2013); and 3) Equatorial Rossby waves and mixed Rossby-Gravity waves in the South Indian Ocean (SI), South Pacific (SP), and Australian (AUS) regions (Hall et al., 2001; Bessafi & Wheeler, 2006; Frank & Roundy, 2006). Other forms of large-scale disturbances favorable for TC formation are the monsoon trough, regions with upper-level troughs and low-level wind surges (Ferreira & Schubert, 1997; Briegel & Frank, 1997; Ritchie & Holland, 1999; Wang & Mognusdottir, 2005, 2006; Zong & Wu, 2014).

Every year a large number of tropical depressions form in global ocean basins from various types of tropical disturbances. However, despite apparently suitable conditions provided by these disturbances, not all the depressions develop into tropical storms. For instance, in the NA, a large number of AEWs form every year, but only around 30% of them develop into tropical storms (Avila, 1991). Understanding of the TC formation pathway has recently been advanced by the "marsupial paradigm" defined within tropical easterly waves over the Atlantic and Pacific regions (Dunkerton et al., 2009). This innovative work recognizes that TCs form in a relatively rare recirculating region called a pouch within a critical layer of the tropical wave under favorable surrounding conditions. A deep pouch from the low to mid-troposphere within an easterly wave maintains an area of closed circulation, where the entry of outside air is restricted, shelters the storm from disruptive influences and enables it to intensify under a favorable environment (Wang et al., 2010a, 2010b; Wang et al., 2012). Asaadi et al. (2016, 2017) found that developing easterly waves appear to propagate as a packet of four to five waves, tilted somewhat northwest-southeast from zonal. Also, of these waves, only one wave is located at the critical latitude (where the mean flow speed equals phase speed of the wave) and in a region of weak potential vorticity gradient, where TC formation can occur. These studies highlighted the role of a deep pouch and the critical latitudes of the easterly waves favorable for TC formation.

Peng et al. (2012) & Fu et al. (2012) examined the environmental differences between developing and non-developing tropical disturbances detected by time filtering technique to extract synoptic-scale disturbances (tropical waves). They noted that thermodynamical conditions are more important across the NA basin, and dynamical conditions are more

critical across the WNP basin. These studies showed that the relative contribution of large-scale variables to TC formation varies between these two basins due to distinctive large-scale disturbances and varying regional environmental conditions. It is, therefore, essential to study differences between developing and non-developing cases across global ocean basins that have diverse environmental conditions and distinct large-scale disturbances to identify the important predictors for TC formation.

There are many other studies on the environmental differences between the developing and non-developing AEWs across the NA basin (Hopsch et al., 2010; Montgomery & Smith, 2010; Davis & Ahijevych, 2012; Komaromi, 2013; Brammer & Throncroft, 2015; Fowler & Galarneau, 2017). These studies highlight the importance of relative flow within AEWs, increased low-level vorticity, vertical shear, and sufficient tropospheric moisture for the development of an initial disturbance. A moist mid-troposphere increases the strength of convective updrafts by decreasing the effect of dry air, which disrupts the deep convection (Nolan, 2007; Smith & Montgomery, 2012; Wang, 2012). Persistent broad-scale, deep convection can then spin up the primary vortex via a system-scale convergence by the in-up-out secondary circulation (Hendricks et al. 2004; Montgomery et al., 2006b; Tory et al., 2006a, 2006b, 2007; Raymond & Sessions, 2007).

Some studies found that moderate shear or easterly shear is favorable for developing cases (Tuleya & Kurihara, 1981, 1982; Zehr, 1992; Zeng et al., 2010). In contrast, enhanced vertical wind shear misaligns the storm which sometimes leads to ventilation, thereby disrupting the intensification process (Riemer et al., 2010; Tang & Emanuel, 2010; Davis & Ahijevych, 2012; Wang et al., 2012; Alland et al., 2017). Other studies showed that abundant

low-level convergence and enhanced mass flux through organized outflow is associated with sustained deep convection in developing cases, with an anticyclonic circulation in the upper levels (McBride & Zehr, 1981; Lee, 1989a, 1989b; Zehr, 1992; Tuleya, 1991; Zhang & Zhu, 2012; Sears & Velden, 2014).

In addition to the above studies on environmental differences, from particle trajectory analysis around the developing storms in the NA basin, Rutherford et al. (2015) identify a protective layer termed the "shear sheath" surrounding the core of the storm that can inhibit shear-induced storm weakening. This shear sheath is a layer of high deformation (that is, a strain-dominated region) that serves to isolate the core from its surroundings. These strain-dominated regions are termed as the rapid filamentation zones, where convection is suppressed, and subsidence is more pronounced (Rozoff and Schubert, 2006). The shear sheath acts as a barrier layer that protects the initial vortex from external influences by obstructing the horizontal inflow of dry air or opposite signed vorticity fields into the core region of developing storms. Rutherford et al. (2015, 2018) found that the development of a tropical depression to a tropical storm has a notable shear-sheath region around the vortex core region.

From the studies above, we note that there are no global studies on the environmental and structural differences between the developing and non-developing circulations. In the current study, we use a phenomenon-based TC detection and tracking scheme to detect the initial circulations and identify the environmental and structural differences across different ocean basins. This TC detection scheme is developed based on the marsupial paradigm of TC formation. It detects the low deformation vorticity regions within the pouch that have the

potential for tropical storm (TS) formation by using a diagnostic (OWZ) along with other environmental variables. This diagnostic is a product of the normalized Okubo-Weiss (OW) parameter and absolute vorticity (Zeta) parameter (Tory et al., 2013a, b; see section 2 for a more detailed description). The Okubo-Weiss Zeta Parameter (OWZP) tracking scheme detects both a TS that is any TC with low-level winds higher than 17 m /s and a tropical depression (TD) that is any TC weaker than a TS. We consider those TDs that become TSs as developing TCs and the remaining TDs non-developers (Tory et al., 2018). This tracking scheme is particularly helpful in the basins where there are no observational aircraft missions for identifying and tracking the initial depressions. Therefore, we perform a basinwide composite analysis on ERA-Interim reanalysis data using these detected circulations to identify the limiting factors for the development of an initial TD.

From the above literature, TC formation from an initial circulation requires a favorable "external environment," such as enhanced vorticity, low-level cyclonic circulation, a moist atmospheric column, and weak to moderate vertical wind shear. As the circulation intensifies, the "internal environment" (the core of the circulation) becomes more favorable: it becomes moister, vorticity amplifies, and the shear-sheath layer around the core strengthens. It is, therefore, difficult to separate the internal and external environment, so a more developed TC looks like it is in a more favorable environment than a weaker TC. By focusing on the differences between developing and non-developing TCs 48 hours before the TD declaration, we have some confidence that most of the differences we identify are likely to be external rather than internal. This composite analysis helps us to find out the external environmental

conditions and structural variations that assist or hinder TS formation, and whether these conditions are similar or differ between ocean basins.

Section 2 of the paper describes the data and methods. Section 3 and 4 provide the results and discussion, respectively, while Section 5 summarizes the conclusions.

2. Data and Methodology

2.1 TS observations and ERA-Interim data

The observed TS information from 1989 to 2018 is from the International Best Track Archive for Climate Stewardship (IBTrACS) database (Knapp et al., 2010). The TS genesis location of IBTrACS is the first position at which the system satisfies a maximum sustained low-level 10 min wind speed higher than 33 knots (17 ms^{-1}) during its lifetime. The reanalysis fields are taken from the ERA-Interim data, compiled by the European Centre for Medium-Range Weather Forecasts (Compo et al., 2011; Dee et al., 2011). These data have a horizontal resolution of $0.75° \times 0.75°$. We extract the data for a period of 30 years, from 1989 to 2018, at 12 hourly intervals (00 and 12 UTC) to create variables used by (i) the TC detector and (ii) the composite analysis of the environmental conditions.

The variables used by the detector at 12 hourly intervals (00 and 12 UTC) include the zonal (u) and meridional (v) wind fields, to compute 1) the OWZ at both 850 and 500-hPa pressure levels (Tory et al., 2013a); 2) vertical wind shear (vector wind difference magnitude) between 850 and 200 hPa pressure levels; and 3) the TC steering velocity (the average wind at 700hPa within a $4° \times 4°$ box region around the grid point center) (Tory et al., 2013a). Additional

parameters include relative humidity at 700 and 500 hPa and 950-hPa specific humidity (SH).

The Okubo Weiss (OW) parameter is a relative measure of vorticity to deformation forces that identifies the rotation dominant regions, along with strain dominated areas such as the shear sheath.

$$OW = \zeta^2 - (E^2 + F^2) \qquad (1)$$

where $\zeta = \left[\frac{\partial v}{\partial x}\right] - \left[\frac{\partial u}{\partial y}\right]$; $E = \left[\frac{\partial u}{\partial x}\right] - \left[\frac{\partial v}{\partial y}\right]$; $F = \left[\frac{\partial v}{\partial x}\right] + \left[\frac{\partial u}{\partial y}\right]$

Here, ζ is the relative vorticity, E and F represent the stretching and shearing deformation respectively.

Tory et al. (2013 a, b) show that the enhanced values of OWZ identify the system-scale low-deformation vorticity regions of solid body rotation. Therefore, the phenomenon-based TC detection and tracking scheme (OWZP) uses the diagnostic variable OWZ which replaces the absolute vorticity variable of other traditional TC tracking schemes. The OWZ calculation involves normalization of the OW parameter by the square of the relative vorticity. The OWZ uses only positive values which include a range of flows, from deformation-dominated flows (OW_{norm} = 0) to rotation dominant regions (OW_{norm} = 1). The phenomenon-based TC tracking scheme uses the thresholds of the OWZ variable instead of the OW variable.

The equation representing the OWZ is:

$$OWZ = \max(OW_{norm}, 0) \times (\zeta + f) \times sign(f) \qquad (2)$$

$$OW_{norm} = \frac{OW}{\zeta^2} \qquad (3)$$

Here OW_{norm} is the normalized OW parameter, and f is the Coriolis parameter.

The variables used to examine the composite storm environment are those already found to be important for TC formation (Gray, 1968; McBride & Zehr, 1981; Emanuel & Nolan, 2004; Camargo et al., 2007; Tippet et al., 2011; Tory et al., 2013a). These variables include the total column water (TCW; in units of kg/m^2), 700 hPa relative humidity (RH; %), maximum potential intensity (MPI; m/s), 850 hPa Relative vorticity (*RVor;* s^{-1}×10^{-6}), 500 hPa Omega (Omega; Pa/s), 200 hPa divergence (DIV*;* s^{-1}×10^{-6}), vertical shear of zonal wind ($U_{200} - U_{850}$) (Ushear; m/s), and OW parameter (s^{-2}×10^{-10}). We consider the positive values of Ushear as westerly shear and negative values as easterly shear. Here, the signs of Omega globally and RVor in the Southern Hemisphere are reversed, meaning that positive Omega is now upward motion, and positive RVor in the Southern Hemisphere is now cyclonic flow. We calculate the MPI using the equation formulated by Bister and Emanuel (1998):

$$MPI = \frac{T_s}{T_o}\frac{C_k}{C_D}\left[CAPE_e - CAPE_b\right] \qquad (4)$$

where T_s is the sea surface temperature, T_o is the outflow temperature, C_k denotes the enthalpy exchange coefficient, C_D denotes the drag coefficient, and *CAPE* is the convectively available potential energy with the subscripts *e* and *b* denoting the environmental and boundary layer atmospheric sounding respectively. In addition to the above large-scale environmental variables, we use a meridional gradient of absolute vorticity (Beta*) variable:

$$Beta^* = \frac{\partial \eta}{\partial x} = \frac{\partial f}{\partial y} + \frac{\partial \zeta}{\partial y} \qquad (5)$$

where η denotes the absolute vorticity. Tory et al. (2018) found that TC formation is favored in regions with lower values of the Beta* and is extremely rare in regions of enhanced values.

2.2 TC detection and tracking

Tory et al. (2013a) found that 95% of observed TSs (IBTrACS) have enhanced values of OWZ at both 850 hPa and 500 hPa levels relative to their surroundings, prompting them to base their OWZP TC tracking scheme on these two quantities along with other variables. The other atmospheric variables are RH at 700 and 950 hPa, specific humidity at 950 hPa, and vertical wind shear. This scheme is designed to be applied to data on a $1° \times 1°$ grid. Therefore, we interpolate the ERA-interim data in the current study to $1° \times 1°$ grid resolution. Tory et al. (2013a, 2013b) give a detailed explanation of the detection scheme, which is a multi-step process:

(i) Detect storms: Identify circulations that have the potential for TC formation by testing every grid point with an initial set of threshold conditions (Table S1 of the supporting information gives the "initial" thresholds). Neighboring grid points satisfying the initial thresholds are clustered into individual clumps that represent the storm at specific times.
(ii) Create storm tracks: Individual storm tracks are constructed by linking the above instantaneous clumps forward in time based on the circulation's expected position from the 700 hPa steering flow, calculated as described in Section 2.1. The tracks cease when there is no future circulation in the vicinity of the expected storm position.
(iii) Detect TCs: Figure 1 gives a schematic diagram of this process. At each point along the storm track, clump averages of different large-scale variables are assigned to each clump

(storm) position. The core thresholds of Table S1 are checked with each clump position and labeled as "True" if the clump satisfies these core thresholds or "False" if not. Each storm track is assessed to see if it satisfies TD status, and then TS status. A particular track is declared a TS (TD) if it satisfies the core thresholds for at least 48 (24) hours consecutively, which amounts to five (three) consecutive true values for 12 hourly data.

Application of the TD and TS detection routine to 30 years of ERA-Interim data yielded 2300 TSs and 3432 TDs. The TD numbers include the 2300 TSs, as all TSs were once TDs. This shows that the TD to TS ratio is about 3:2, implying globally there are 50% more lows that satisfy the TD than the TS thresholds, which is consistent with the 1979-2013 period considered by Tory et al. (2018). To obtain the non-developing depressions, we subtract the developed depressions (TSs) from the total tropical depression (TD) dataset. A total of 1132 non-developing storms are detected, located across all the ocean basins. The fifth True position along the track of the TS (Figure 1) is considered as the TS genesis which matches with the IBTrACS genesis position in most of the ocean basins (Bell et al., 2018) whereas third true position is considered as the TD genesis. Tory et al. (2018) tuned the OWZP scheme to detect the TDs in the tropical disturbance dataset across the Australian region. Also, Bell et al. (2018) assessed the pre-genesis tracks of the OWZP and IBTrACS TSs and noted that OWZP detected TSs have earlier tracks with longer duration because the scheme detects the locations that have potential for TS formation rather than the matured TSs.

2.3 Storm-centered spatial composites of developing and non-developing cases

To understand the environmental differences between developing and non-developing TDs, storm centered composites of the environmental variables are created within a 24° ×24° region around the depression center. Also, we calculated the streamlines of the composite storm overlaid with the OW parameter and RH contours to understand the structural differences and the influence of the surrounding environment on the initial circulation. We include only the storms with a detected storm track that existed 48 hours before TD declaration. This group contains developing (PDV48) and non-developing storms (PND48) across each ocean basin (Table S2 shows basin boundaries). The analysis considers three periods: 48 and 24 hours before the time of TD formation, and the day of TD declaration, labeled Day-2, Day-1, and Day0, respectively as shown in Figure 1.

2.4 Statistical Index:

To quantify the differences in the environmental conditions between the developing and non-developing TDs, we calculate the Box Difference Index (BDI) (Peng et al., 2012) for PDV48 and PND48 cases across all the ocean basins within a 12°×12° box region around the depression center (blue boxes in Figure S1 in the supplementary section). This domain size appears to show the maximum differences between developing (DV) and non-developing (ND) compared to the 24°× 24° region which covers a larger spatial extent and may disrupt the box averages. The OW variable which includes the vorticity dominated and shear-sheath regions is divided into two variables. For this we use a 9°×9° box region (green boxes in Figure S1), the “OW center” variable uses the centered box showing the low-deformation vorticity strength and the “OW surrounding” variable determines the strength of the shear sheath uses the remaining boxes. The BDI index is defined as:

$$BDI = \frac{mean(DV) - mean(ND)}{std(DV) + std(ND)} \qquad (6)$$

where *mean(DV)* and *mean(ND)* are the mean of the environmental variables for DV and ND cases and *std(DV)* and *std(ND)* are the standard deviation of the DV and ND environmental variables respectively. The higher the magnitude of the BDI (which ranges from 0 to 1), the better the variable can differentiate the two cases. The sign of the BDI index tells us the environmental behavior of the variable. In general, positive values indicate that the quantity favors development. However, the opposite is true for quantities in which small values favor TC formation, such as Ushear, Beta* and OW surrounding variables. The negative values of Ushear, Beta* and OW surrounding variables indicates favorable shear, barotropic stability regions and stronger shear sheath regions respectively that supports the TC formation. We use a two-sample t-test to determine the statistical significance of the differences between DV and ND cases.

3. Results

This section describes the storm-centered composite analysis of initial circulations that exists two days before TD declaration to identify structural differences and key limiting variables across each ocean basin that lead to the non-development of an initial circulation.

3.1 Geographical distribution of TS and TD genesis locations:

Figure S2 shows the geographical distribution of genesis locations of IBTrACS and OWZP detected DV and ND depressions using the ERA-interim reanalysis. The genesis dots of the IBTrACS and the OWZP detected TSs have similar geographical locations in most of the

ocean basins. Tory et al. (2013b) statistically tested the performance of this TC detection scheme when compared with the IBTrACS for 20 years from 1989-2008. They showed globally 78% of IBTrACS storms are correctly detected using this scheme with a 25% false alarm rate. Also, of all the ocean basins the NI basin has poor performance, perhaps due to the NI being a unique land-enclosed basin and mis-identification of the monsoon lows as TCs. We perform a basin-wide analysis of the mean annual frequency bias of the OWZP detected storms and IBTrACS for the 30 years 1989-2018. Table S3 shows that the NA, ENP, and SP basins have underpredicted genesis compared to observations. These negative biases across the ENP, NA, and SP basins may be due to more short-lived and land influenced storms compared to the WNP and SI basins that have more long-lived storms over the open ocean waters, which are usually detected well by the OWZP scheme (Tory et al., 2013b).

3.2 Structural differences between developing and non-developing tropical depressions:

Typically, a TS has a developed vortex core region from low to mid-level with cyclonic circulation along with anticyclonic outflow at upper levels associated with a secondary circulation (McBride and Zehr, 1981; Dunkerton et al., 2009; Wang et at., 2012). Addtionally, developing cases have a stronger shear-sheath layer from the low to mid-troposphere around the core of the storm. This shear sheath protects the vortex core region from external influences like the horizontal intrusions of drier air or lower values of opposite sign vorticity (Rutherford at al., 2015, 2018). Therefore structural variations, along with spatial distribution of environmental variables, are explored in detail 48 hours before TD declaration using spatial composites within a 24° ×24° box region around the depression center across all the ocean basins. This box region covers a larger spatial extent including the

centered cyclonic circulation and the surrounding region which helps us to understand the influence of external environment on the circulation.

3.2.1 Northern hemisphere (NH) basins:

We examine the spatial composites of the atmospheric variables evolving from Day-2 to Day0 to differentiate the DV and ND cases across the NA basin. The differences in the spatial composites of relative humidity (RH) between the DV and ND cases in Figure 2a illustrate that developing cases have higher moisture at the center and surrounding regions compared to the non-developing cases from lower (850 hPa) to mid-troposphere (500 hPa). Also, the DV cases have fully enclosed streamlines around the center at 500 hPa shown in Figure 4, whereas in ND cases streamline gradually diverge to the northwest of the center on Day0 with dry air surrounding the core region in the northwest side. Figure 2b indicates that ND cases have unfavorable shear at the center and surrounding compared to the DV cases as it propagates from Day-2 to Day0 (Figure 5a shows averaged values of Ushear). The negative values of Uhsear indicate that ND cases have either stronger westerly shear (positive values) or weaker easterly shear (lower negative values). Also, Figure 2c shows that DV cases have increasing values of DIV from Day-2 to Day-0 at the center and surrounding regions compared to the ND cases indicating the development of stronger outflow jet associated with sustained convection in the DV cases. Similarly, Figure 2d shows that DV cases have higher values of MPI at the center and surrounding regions compared to the ND cases indicating greater thermodynamic instability in DV cases.

We further examine the spatial composites of the OW parameter overlaid with streamlines in the co-moving frame of the composite storm for both PDV48 and PND48 cases over the NA basin at 850, 700, 500, and 200 hPa levels. Figure 3 and Figure 4 shows that closed or nearly closed streamlines surround the cyclonic cores from low to mid-levels of the atmosphere. Each cyclonic circulation has a core of positive OW (strain-free rotation) surrounded by a band of negative OW (higher lateral strain, indicating the shear sheath), which extends from the lower (850 hPa) to the middle troposphere (500 hPa). A general decrease in the size and strength of the cyclonic circulation with height is evident, culminating in stronger anticyclonic outflow streamlines to the east of the center at 200 hPa for developing cases (Figure 4). In order to understand quantitatively the strength of centered circulation and the surrounding shear-sheath in the DV and ND cases we use box averages of the OW center and OW surrounding parameters (Table S4 and S5) as described in section 2.4. The OW center values of non-developing cases show that the cyclonic circulation is significantly weaker than in the developing cases (Table S4). The OW surrounding values shows a development of a more pronounced shear-sheath (higher negative OW values) in DV cases on Day0 at both lower and mid-levels (Table S5). The stronger the circulation, the stronger the OW core, and the stronger the shear sheath develops in DV cases.

As the depression develops, a stronger shear sheath layer forms in the north, east, and west side of the storm center enclosing the core region in the developing cases. This layer offers higher resistance for the surrounding dry air or opposite signed vorticity to penetrate towards the center. In contrast, non-developing cases have a weaker shear sheath layer enclosing a smaller area around the vortex center at 700 and 500 hPa levels (Figure 3 & 4), with a

relatively weaker layer on the west side of the storm. The non-developing cases in Figure 4 show an intrusion of dry air at the 500 hPa level (as indicated by the 50% RH values in black contour) into the vortex core region on day0 from the northwest side of the depression may be due to weaker shear sheath layer. Also the Figure 5a shows that there is an increased mean westerly shear in the ND cases as the circulation approaches Day0. Shu et al. (2014) noted that westerly shear is detrimental to the development of a TC as it draws in cold, dry air from the poleward side of the storm. Brammer and Thorncroft (2015) noted that moisture in the north and northwest side is an important factor for developing storms from AEWs. Therefore a less protective vortex having a weaker shear-sheath layer particularly in the northwest side of the center, westerly shear, and lower atmospheric moisture content leads to the non-development of initial TDs in the NA basin.

A similar spatial composite analysis is performed in other NH basins (ENP, WNP, WNP_P), as shown in Figure S3, Figure S4, and S5. We separate the WNP basin into equatorward WNP (0-15N) and poleward WNP_P (15-30N) regions due to different TD failure rates (Tory et al., 2018). These basins also show that ND cases have weaker shear sheath layers leading to dry air intrusion due to weak mean easterly shear (except in WNP) shown in Figure 5 (b, c, d), thereby disrupts the deep convection suppressing the development of initial depression. Also, the box-averaged values of OW center and OW surrounding variables show that DV cases have higher positive centered core region with a stronger negative surrounding shear sheath (Table S4 and S5). In the NI basin (Figure S6), the non-developing cases have disorganized circular structure of the centered positive OW core region at middle levels of the troposphere with significantly lower magnitude on Day0 (Table S4). Also, the ND cases

across the NI basin have weaker shear sheath layer at mid-levels (500hPa) on Day0 but do not indicate the mid-level dry air intrusion into the center due to favorable mean easterly shear (Figure 5e). Therefore, a lack of organized structure of centered circulation in the ND cases leads to the non-development of the circulation across the NI basin.

3.2.2 Southern Hemisphere (SH) basins

The spatial composites of the atmospheric variables in the SH indicate a larger spatial extent with a higher magnitude of these variables in DV cases compared to the ND cases (not shown). Figures S7, S8, and S9 show the OW composites overlaid with the streamlines over the SI, SP, and AUS basins, respectively. These basins also depict similar structural features as observed in the NH basins with a stronger cyclonic circulation at low-levels and anti-cyclonic at upper levels. The DV cases have significantly higher OW center values and a stronger shear sheath with stronger negative OW surrounding values from the low (850 hPa) to mid-troposphere (500 hPa) (Table S4 and S5). The ND cases have weaker mean easterly shear or increased westerly shear (Figure 5g, h) in SP and AUS basins compared to the DV cases. In contrast, the SI basin has similar mean shear for both DV and ND cases (Figure 5f). Across these ocean basins, the non-developing cases have a weaker shear-sheath layer on the west side of the depression indicating mid-level dry air intrusion (with 55-60 % RH values) to the center of the depression impeding the development of TD. Therefore a less protected vortex having a weaker shear-sheath layer with unfavorable shear disrupts the intensification of the initial circulation to a TS.

3.3. Quantification of differences from statistical distributions using the BDI

We computed the statistical distributions of the environmental variables averaged within a $12^{o} \times 12^{o}$ box region on Day-2, Day-1, and Day0 to reveal the variables that show significant differences between the DV and ND cases (Figure S10 to S13). Although statistical distributions identify the variables showing significant differences between DV and ND cases, they do not give the order of the important variables. The BDI index, which uses the mean and standard deviation of the samples, describes the relative importance of variables in distinguishing DV from ND and is calculated for each large-scale variable on Day-2, Day-1, and Day0. In particular, this index identifies which quantities/processes are most detrimental to TS formation. Here, we use both Day-2 and Day0 BDI values to rank the order of prominent variables (Table 1), including their statistically significance, that hinder/favor the intensification of an initial circulation. The BDI values of 700 hPa RH correlate with TCW, and BDI values of Omega correlate with DIV across all the ocean basins, therefore we include only TCW and Omega in the BDI discussion.

3.3.1 NH basins:

Across the NA basin, Figure 6a shows that as the DV circulation approaches Day0, we observe increased updrafts (Omega) and low-level vorticity (RVor) suggesting a developing circulation due to availability of sufficient tropospheric moisture (TCW) from Day-2. This higher moisture favors sustained convection by increasing the efficiency of upward mass flux and thereby increases the strength of the circulation. Also, as the circulation approaches Day0, we observe that DV cases have favorable mean shear compared to the ND cases that

have mean westerly shear (Figure 5a). The lower values of moisture and unfavorable shear leads to disruption of deep convection that suppresses the development in ND cases. Also, the BDI values show that DV cases have higher thermodynamical instability measured in terms of MPI. This analysis shows that tropospheric moisture is an important limiting factor across this basin for an initial circulation to develop into a TS. A few studies noted that the Saharan Air Layer (SAL) acts as a modulating influence for the TC activity across this basin. As it suppresses the convection, entrains dry air to the center of the circulation, and increases vertical wind shear leading to non-development of the circulation (Dunion & Veldon, 2004). Other studies noted that pre-existence of a dry troposphere or the advection of the dry air by the AEWs, large-scale subsidence, TC-TC interactions or TC interaction with environment creates a dry atmosphere and higher vertical wind shear that disrupts storm formation (Hopsch et al., 2010; Braun, 2010; Brammer & Thorncroft, 2015; Fowler & Galarneau, 2017). Therefore, the availability of sufficient tropospheric moisture around the disturbance with favorable shear supports the development of the incipient circulation.

From the BDI values across the ENP basin (Figure 6b), as the circulation progresses from Day-2 to Day0, DV cases have increased TCW at the center and surrounding of the circulation along with favorable mean easterly shear (Ushear) compared to the ND cases (Figure 5b). The lower BDI values of RVor indicate that both DV and ND cases have similar low-level vorticity. Therefore, the lack of sufficient tropospheric moisture and unfavorable shear suppresses the development of an ND case across the ENP basin. The limiting variables for TS formation identified from this analysis also agree with other studies at different

timescales. For instance, at interannual timescales across the ENP basin, Zhao and Raga (2015) noted that mid-level relative humidity acts as a significant contributor to TS formation in inactive years (i.e., years observed with low TC activity) and vertical wind shear is the most important parameter in the active years (high TC activity).

The WNP basin is the most active basin for TC formation across the global ocean basins due to favorable regional environmental conditions. There is a strong monsoon circulation that provides sufficient low-level convergence and higher SSTs due to the warm pool region favor TC formation. Nevertheless, there exist environmental differences between DV and ND cases due to the prevalence of different synoptic-scale disturbances across the basin (Li, 2006; Li & Fu, 2006; Fu et al., 2012). The higher BDI values from Figure 6c and 6d shows that DV cases have stronger vorticity (RVor) and increased updrafts (Omega) compared to the ND cases. These higher values of vorticity in DV cases from Day-2 indicate that the initial circulation originated in a strongly convective region, which favors further intensification by deep convection. Also, the thermodynamic favorability measured in terms of MPI and TCW is higher for DV cases compared to the ND cases across the entire basin. In addition, across the WNP_P basin, DV cases have favorable mean easterly shear (Ushear) compared to the ND cases (Figure 5d). The initial circulation originating in a weakly convective region with a less thermodynamically unstable environment leads to the non-development across the basin. Therefore, the dynamical condition is more important for the development of an initial circulation across the WNP basin (McBride& Zehr, 1981; Lee, 1989 a, b; Fu et al., 2012). Across the NI Ocean, from the BDI values of Figure 6e, we observe that DV cases have stronger updrafts (Omega) on Day0 compared to the ND cases. A study by Tsuboi and

Takemi (2014) noted that Omega acts as a major contributor the changes in the TC frequency during the active phase of the Madden-Julian Oscillation (MJO) across this basin. The NI Ocean is a unique basin compared to other basins as it doesn't observe significant differences for most of the large-scale variables perhaps due to poor performance of TC frequency characteristics using the OWZP scheme (Tory et al., 2013b).

3.3.2 SH basins:

The BDI analysis over the SH basins show some similarities with the NH basins in the significant limiting variables with a difference in the order of the variables (Table 1). Figure 6f shows that the DV cases in SI Ocean has higher TCW, Omega and RVor compared to the ND cases. Over the SP basin, the BDI values in Figure 6g show that DV cases have favorable thermodynamic conditions and mean easterly shear compared to the ND cases (Figure 5g). Therefore both thermodynamical (MPI & TCW) and dynamical (Ushear) conditions act as the significant influencing variables for the development of a TD across the SP basin. From the BDI values across the AUS basin (Figure 6h), we observe that DV cases have higher RVor and TCW compared to the ND cases. Also, the DV cases have favorable mean easterly shear compared to ND cases (Figure 5h). Earlier studies at different time scales show that sea surface temperatures, vertical wind shear, RH, and RVor are significant influencing variables across SH basins (Camargo et al., 2007; Ramsay et al., 2008; Kuleshov et al., 2009; Chand & Walsh, 2011; Dowdy et al., 2012; Liu & Chan, 2012).

In addition to the above large-scale variables, we estimate the BDI index of the Beta*, OW center, and OW surrounding variables across these ocean basins. The Beta* variable which shows the barotropic instability regions is found to differentiate the DV and ND cases across

the ENP and SP basins. Also, from the BDI index values of the OW center variable (Figure 7), we observe that developing cases have higher magnitudes of OW center across all the ocean basins, indicating strong low-deformation vorticity regions. Also, the BDI values of OW surrounding variable (Figure 7) show that DV cases have stronger negative values compared to the ND cases in most of the ocean basins indicating a stronger shear-sheath that protects the vortex from external negative influences. Therefore, in addition to the above large-scale variables, the Beta*, OW center, and OW surrounding parameters can be used as predictors across the ocean basins to discriminate the DV and ND cases.

4. Discussion:

The circulation centered spatial composites of the RH, DIV, and MPI variables evolving from Day-2 to Day0 show that developing cases have more considerable spatial extent surrounding the vortex core of a region of the higher magnitude of these variables (Figure 2). In contrast, the non-developing cases have less spatial extent and lower values of the environmental conditions from Day-2. The Ushear spatial composites show that non-developing cases have either strong mean westerly shear or weak easterly shear unfavorable for TS formation. The composites of the streamlines overlaid with shaded OW parameter and RH contours help us to identify the structural variations between DV and ND cases (Figure 3 & 4). These composites show that non-developing cases have lower values of centered OW along with a weaker band of negative OW values (the shear sheath) surrounding the core region from lower-levels to mid-levels compared to the DV cases across most of the basins (Table S4 & S5). In contrast, developing cases have stronger OW core regions and a stronger surrounding shear sheath layer from lower to mid-levels. Also, DV cases have mean easterly wind shear,

which draws the warm moist air from the equatorward side of the storm (Shu et al., 2014). In ND cases, the increased westerly shear or weak easterly shear, as well as a weaker shear sheath in the west or northwest side of the vortex center on day0, may lead to horizontal entrainment of surrounding drier air at mid-troposphere (500 hPa) in some of the basins. Drawing the cold, dry air from the side with a weaker shear-sheath layer may disrupt the storm formation in ND cases by reducing the overall moisture content and affecting the sustained convection. In contrast to the above results, across the NI basin, both DV and ND cases have easterly shear and weaker shear sheath region. However, an unorganized structure of the OW centered values leads to the non-development of the initial circulation in this basin. Therefore, a more compact vertical structure from lower levels to mid-levels with a stronger centered vortex along with a stronger shear-sheath layer protects the incipient circulation.

The BDI index illustrates the relative importance of the thermodynamical and dynamical conditions on the development of TS from an initial circulation. The BDI magnitude (Figure 6 & Figure S14) from day-2 to day0 shows that environmental differences between DV and ND gradually increase from Day-2 to Day0. These differences indicate that either DV cases are in favorable environmental conditions or there is the increased influence of destructive forces in ND cases. Table 1, which shows the order of important variables, notes slight differences in the order of these influencing variables on day-2 and day0, with similar environmental variables appearing to be prominent on both days but with a larger magnitude on day0. Figure 6 gives an overview of the role of environmental variables on the development of an initial circulation from the BDI values. It shows some agreement between

the global ocean basins. For instance, TCW, RVor, and Omega variables show significant differences between DV and ND cases with a higher magnitude of BDI index in almost all the ocean basins. In contrast, MPI, Ushear, and Beta* show differences and seem to play a role in fewer ocean basins.

Although the current analysis does not illustrate the precise convective processes leading to the development of a TS, Figure 6 shows that the DV cases have higher moisture over different ocean basins indicated by positive BDI values of TCW. The higher tropospheric moisture favors sustained deep convection that leads to a strong low to mid-level vorticity concentration due to increased convective heating (Wang et al., 2012; Wang, 2014). In contrast, the ND cases that has drier troposphere lead to weaker deep convection due to weaker updrafts and downdrafts (James & Markowski, 2009; Kilroy & Smith, 2013). Some earlier studies noted that the thermodynamical variable MPI is a vital predictor to determine the TS formation using statistically derived genesis potential indices (Emanuel & Nolan, 2004; Bruyère et al., 2012). This MPI acts as one of the significant influencing factors across the WNP, WNP_P, NA, SP, and AUS basins indicating favorable thermodynamic instability in developing cases.

In the examination of the dynamical variables, Figure 6 shows that the ND cases have lower values of RVor and Omega across all the ocean basins except over the ENP and the NI (Fig 6). The higher magnitudes of RVor and Omega indicates sustained convection and abundant low-level convergence, favorable for TS formation (Tory & Frank, 2010; Montgomery & Smith, 2010). Also, ND cases have weaker mean easterly shear or increased westerly shear across the ocean basins except in the WNP (0-15N), NI, and the SI basins (Figure 5),

indicating that weak mean easterly shear or increased westerly shear may be detrimental to TS formation. Ritchie and Frank (2007) showed that easterly shear could offset the northwesterly shear induced by the vortex due to the beta effect as the possible reason for westerly shear being detrimental to development. In contrast to the above differences, there are no significant environmental differences between DV and ND cases across the NI basin except for Omega. The BDI analysis shows some similarities between the ocean basins with similar prominent variables. However, the order of these variables varies from basin to basin, perhaps due to distinct large-scale disturbances, different modulating influences and differences in the background environmental conditions. Also, DV cases have higher positive BDI values of OW center variable and higher negative BDI values of OW surrounding variable favorable for TS formation in most of the basins (Figure 7). Therefore, observing the OW values at the center and surrounding the circulation center from low to mid-troposphere in numerical weather prediction models or including the OW center and OW surrounding variables in statistical models may improve the forecast accuracy of the TS formation from a depression stage vortex.

5. Conclusion:

The differences in the large-scale disturbances and the mean flow conditions across the global ocean basins may lead to differences in the relative contribution of large-scale variables to TS formation. Therefore, in this study, we perform a basinwide statistical analysis on the environmental differences between developing and non-developing depressions by following the depression two days before its declaration in a Lagrangian manner. We use a previously developed TC detection technique to detect both developing

and non-developing tropical circulations in the ERA-Interim reanalysis. The spatial composites of atmospheric variables and streamlines from Day-2 to Day0 help us to monitor the evolving flow features around the depression in each ocean basin. We employ a statistical BDI index to quantitatively identify the order of important atmospheric variables that distinguish the developing and non-developing depressions across each ocean basin. We find the following main conclusions:

- The spatial composites of the environmental variables show that DV cases have more favorable conditions at the center and surrounding compared to the non-developing cases from two days before TD declaration (Figure 2).
- The DV cases have a protective vortex with a strong positive OW core region and the development of a surrounding region of stronger negative OW, the "shear sheath," from the low to mid-troposphere as it approaches TD declaration stage (day0). In contrast, non-developing cases have less protective vortex with a weaker shear sheath in the northwest/west side of the depression leading to the intrusion of cold, dry air to the center of the circulation at mid-levels (500 hPa) on day0 (Figure 3 & 4).
- The ND cases have either mean westerly shear or weaker mean easterly shear in few ocean basins (Figure 5), which leads to dry air intrusion disrupting the intensification of the vortex.
- Based on the BDI values on day-2 and day0 (Table 1), TCW and RVor act as significant limiting factors for TS formation over the NA; RVOR over the WNP basins; TCW, and Ushear over the ENP basin; and Omega over the NI basin. In SH, TCW, and Omega act as main limiting factors for TS formation over the SI; Ushear,

and MPI over the SP; and RVor and TCW over the AUS basin. This BDI analysis shows that TCW and RVor are important in most of the ocean basins and Ushear, which shows the large-scale influence is prominent in a few ocean basins (Figure 6).

- The BDI values of the OW center and OW surrounding variables show that DV cases have stronger core and stronger shear sheath from Day-2 compared to the ND cases in most of the ocean basins (Figure 7).

This study provides a set of large-scale environmental conditions that act as limiting factors for the development of an initial TD to TS across each ocean basin. We observe similar structural differences between developing and non-developing TDs across most of the ocean basins. In contrast, there are varying contributions of environmental variables that may be due to the distinct large-scale disturbances and their interactions with the basin's mean flow conditions. This study identifies additional predictors for the TS formation forecast in addition to earlier large-scale variables. Therefore, the inclusion of both OW center and OW surrounding variables in building statistical forecast models of TS formation from the initial depressions along with other atmospheric variables such as TCW, MPI, RVor, Omega, Ushear may improve TS forecasts at the synoptic scale. Future work focuses on the application of this methodology to forecast analysis fields to observe whether similar large-scale variables act as impediments for the TS formation from an initial circulation and establish a statistical TS formation forecast model. Also, more detailed analysis will be necessary to understand the variations in the order of important variables across the global ocean basins which improves our understanding of the relationship between large-scale environmental variables and TS formation.

Acknowledgments

We acknowledge valuable discussions with Kevin tory and the constructive comments of three anonymous reviewers. We are grateful to the financial support for the Ph.D. from the

Melbourne India Post-graduate Program. We thank the National Computational Infrastructure System, supported by the Australian Government, for providing the pre-processed ERA-Interim data and computational resources. The authors are thankful for the Australian Research Council Centre of Excellence for Climate Extremes and Earth Systems and Climate Change Hub of the National Environmental Science Program for supplying partial financial support. The ERA-Interim reanalysis data used for current analysis is available at the following link (https://apps.ecmwf.int/datasets/data/interim-full-daily/levtype=pl/).

Figure and Table captions:

Table 1: The order of importance of variables in each ocean basin based on the statistically significant values at the 95% significance level of the BDI index at Day-2 and Day0 (the day of TD declaration).

Figure 1. Diagram showing the tracks of developing and non-developing tropical depressions with F(False) indicating that the core thresholds are not satisfied and T(True) where the thresholds are satisfied. The 3rd consecutive true is the TD declaration time for both developing and non-developing TDs. Path A shows that all TSs were once TDs, and path B is a TD that did not develop into TS.

Figure 2. Differences in spatial composites of developing and non-developing cases (DV minus ND) within the $24° \times 24°$ box region region around the circulation center over the North Atlantic basin, (a) 850 and 500 hPa RH, (b) Ushear, (c) DIV and (d) MPI. The stippling indicates the 95% significance level differences.

Figure 3. OW overlaid by streamlines computed in a co-moving frame for DV and ND cases at 850 and 700hPa over the North Atlantic basin. The x and y-axis indicating the distance from the center in degrees, the red and magenta contours indicate 80% and 70% RH, respectively and stippling indicates the 95% significance level differences between DV and ND cases.

Figure 4. The same as Figure 3 over the 500 and 200 hPa, the black contour indicate the 50% RH.

Figure 5. Box-plots of averaged Ushear for DV and ND cases within a 12°×12° box region. The horizontal line of the box indicates median of the distribution, the left, and right box edges show 75th and 25th percentiles, the whiskers indicate maximum and minimum values and the red crosses indicate outliers. The statistical significance of Ushear is given in Figure 6.

Figure 6. Basinwide BDI index of environmental variables for PDV48 and PND48 cases on Day-2, Day-1, and Day0. Positive values of the BDI index for TCW, MPI, RVor, and Omega indicate more favorable conditions for development. In contrast, negative values of Ushear, Beta* are more favorable (* indicates a 95% significance level). For parameterwise comparison of the BDI values refer to the Figure S14.

Figure 7. Basinwide BDI index of OW center and OW surrounding for DV and ND cases at 850 and 500 hPa levels on Day-2, Day-1, and Day0. Positive values of OW center variable and negative values of OW surrounding variable are more favorable for TS formation (* indicates a 95% significance level).

References

Alland, J.J., B.H. Tang, and K.L. Corbosiero (2017), Effects of midlevel dry air on development of the axisymmetric tropical cyclone secondary circulation. *J. Atmos. Sci.*, *74*(5), 1455-1470.

Asaadi, A., G. Brunet, and M.K., Yau (2016), On the dynamics of the formation of the Kelvin cat's-eye in tropical cyclogenesis. Part I: Climatological investigation. *J. Atmos. Sci.*, *73*(6), 2317-2338.

Asaadi, A., G. Brunet and M.K. Yau (2017) The Importance of Critical Layer in Differentiating Developing from Nondeveloping Easterly Waves. *J. Atmos. Sci.*, *74*(2), pp.409-417.

Avila, L.A. (1991), Atlantic tropical systems of 1990. *Mon. Weather Rev.*, *119*(8), 2027-2033.

Bell, S.S., S.S. Chand, K.J. Tory, and C. Turville (2018), Statistical assessment of the OWZ tropical cyclone tracking scheme in ERA-Interim, *J. Clim.*, *31*, 2217-2232.

Bessafi, M., and M.C. Wheeler (2006), Modulation of south Indian Ocean tropical cyclones by the Madden–Julian oscillation and convectively coupled equatorial waves. *Mon. Weather Rev.*, *134*(2), 638-656.

Bister, M. and K.A. Emanuel (1997), The genesis of Hurricane Guillermo: TEXMEX analyses and a modeling study. *Mon. Weather Rev.*, *125*(10), 2662-2682.

Bister, M., and K. A. Emanuel (1998), Dissipative heating and hurricane intensity. Meteor. Atmos. Phys., 50, 233–240.

Brammer, A. and Thorncroft (2015), Variability and evolution of African easterly wave structures and their relationship with tropical cyclogenesis over the eastern Atlantic. *Mon. Weather Rev.*, *143*(12), 4975-4995.

Braun, S.A. (2010), Reevaluating the role of the Saharan air layer in Atlantic tropical cyclogenesis and evolution. *Mon. Weather Rev., 138(6),* 2007–2037.

Briegel, L.M., and W.M. Frank (1997), Large-scale influences on tropical cyclogenesis in the western North Pacific. *Mon. Weather Rev.*, *125*(7), 1397-1413.

Bruyère, C.L., G.J. Holland, G.J. and E. Towler (2012), Investigating the use of a genesis potential index for tropical cyclones in the North Atlantic basin. *J. Climate*, *25*(24), 8611-8626.

Camargo, S.J., K.A. Emanuel, and A.H. Sobel (2007), Use of a genesis potential index to diagnose ENSO effects on tropical cyclone genesis. *J. Climate*, *20*(19), 4819-4834.

Camargo, S.J., M.K. Tippett, A.H. Sobel, G.A. Vecchi, G.A. and M. Zhao, M (2014), Testing the performance of tropical cyclone genesis indices in future climates using the HIRAM model. *J. Climate*, *27*(24), 9171-9196.

Chand, S.S., and K.J. Walsh (2011), Forecasting tropical cyclone formation in the Fiji region: A probit regression approach using a Bayesian fitting. *Weather Forecast.*, *26*(2), 150-165.

Compo, G.P., J.S. Whitaker, P.D. Sardeshmukh, N. Matsui, R.J. Allan, X. Yin, B.E. Gleason, R.S. Vose, G. Rutledge, P. Bessemoulin, and S. Brönnimann (2011), The twentieth century reanalysis project. *Q. J. Roy. Meteorol. Soc.*, *137*(654), 1-28.

Davis, C.A. and D.A. Ahijevych (2012), Mesoscale structural evolution of three tropical weather systems observed during PREDICT. *J. Atmos. Sci.*, *69*(4), 1284-1305.

Dee, D.P., S.M. Uppala, A.J. Simmons, P. Berrisford, P. Poli, S. Kobayashi, U. Andrae, M.A. Balmaseda, G. Balsamo, D.P. Bauer, and P. Bechtold (2011), The ERA-Interim reanalysis: Configuration and performance of the data assimilation system. *Q. J. Roy. Meteorol. Soc.*, *137*(656), 553-597.

Ditchek, S.D., T.C. Nelson, M. Rosenmayer, and K.L. Corbosiero (2017), The Relationship between Tropical Cyclones at Genesis and Their Maximum Attained Intensity. *J. Climate*, *30*(13), 4897-4913.

Dowdy, A.J., L. Qi, D. Jones, H. Ramsay, R. Fawcett, and Y. Kuleshov (2012), Tropical cyclone climatology of the South Pacific Ocean and its relationship to El Niño–Southern Oscillation. *J. Climate*, *25*(18), 6108-6122.

Dunion, J. P., and C. S. Velden (2004), The impact of the Saharan Air Layer on Atlantic tropical cyclone activity. *Bull. Amer. Meteor. Soc., 85(3),* 353-365.

Dunkerton, T.J., M.T. Montgomery, and Z. Wang (2009), Tropical cyclogenesis in a tropical wave critical layer: Easterly waves. *Atmos. Chem. Phys., 9*(15).

Emanuel, K. and D.S. Nolan (2004), Tropical cyclone activity and the global climate system. *Extended Abstracts, 26th Conf. on Hurricanes and Tropical Meteorology*, Miami, FL, Amer. Meteor. Soc., 240–241.

Ferreira, R.N., and W.H. Schubert (1997), Barotropic aspects of ITCZ breakdown. *J. Atmos. Sci., 54*(2), 261-285.

Fowler, J.P. and Galarneau Jr, T.J., 2017. Influence of storm–storm and storm–environment interactions on tropical cyclone formation and evolution. *Mon. Weather Rev., 145*(12), 855-4875.

Frank, W.M., and P.E. Roundy (2006), The role of tropical waves in tropical cyclogenesis. *Mon. Weather Rev., 134*(9), 2397-2417.

Fu, B., Li, T., M.S. Peng, and F. Weng (2007), Analysis of tropical cyclogenesis in the western North Pacific for 2000 and 2001. *Weather Forecast., 22*(4), 763-780.

Fu, B., M.S. Peng, T. Li, and D.E. Stevens (2012), Developing versus nondeveloping disturbances for tropical cyclone formation. Part II: Western North Pacific. *Mon. Weather Rev., 140*(4), 1067-1080.

Gray, W.M. (1968), Global view of the origin of tropical disturbances and storms. *Mon. Weather Rev.*, 110, 548-586.

Gray, W. M. (1975). Tropical cyclone genesis. Atmos. Sci., 234 pp.

Hall, J.D., A.J. Matthews, and D.J. Karoly (2001), The modulation of tropical cyclone activity in the Australian region by the Madden–Julian oscillation. *Mon. Weather Rev.*, *129*(12), 2970-2982.

Hendricks, E.A., M.T. Montgomery, and C.A. Davis (2004), The role of "vortical" hot towers in the formation of tropical cyclone Diana (1984). *J. Atmos. Sci.*,*61*(11), 1209-1232.

Hennon, C.C., and J.S. Hobgood (2003), Forecasting tropical cyclogenesis over the Atlantic basin using large-scale data. *Mon. Weather Rev.*, *131*(12), 2927-2940.

Hopsch, S.B., C.D. Thorncroft, and K.R. Tyle (2010), Analysis of African easterly wave structures and their role in influencing tropical cyclogenesis. *Mon. Weather Rev.*, *138*(4), 1399-1419.

James R. P., P.M. Markowski., (2009), A numerical investigation of the effects of dry air aloft on deep convection. *Mon. Weather Rev.*,138, 140-161.

Jones, S.C. (1995), The evolution of vortices in vertical shear. I: Initially barotropic vortices. *Q. J. Roy. Meteorol. Soc*., 121(524), 821-851.

Kilroy, G. and R.K. Smith, (2013), A numerical study of rotating convection during tropical cyclogenesis. *Q. J. Roy. Meteorol. Soc.*, 139, 1255-1269.

Knapp, K.R., M.C. Kruk, D.H. Levinson, H.J. Diamond, and C.J. Neumann (2010), The international best track archive for climate stewardship (IBTrACS) unifying tropical cyclone data. *Bull. Am. Meteorol. Soc.*, *91*(3), 363-376.

Komaromi, W.A. (2013), An investigation of composite dropsonde profiles for developing and nondeveloping tropical waves during the 2010 PREDICT field campaign. *J. Atmos. Sci.*, *70*(2), 542-558.

Kuleshov, Y., F. Chane-Ming, L. Qi, I. Chouaibou, C. Hoareau, and F. Roux (2009), Tropical cyclone genesis in the Southern Hemisphere and its relationship with the ENSO. *Ann. Geophys.* (Vol. 27, No. 6, 2523-2538).

Landsea, C. W. (1993), A climatology of intense (or major) Atlantic hurricanes. *Mon. Weather Rev.*, 121, 1703–1712.

Lee, C.S., R. Edson, and W.M. Gray (1989), Some large-scale characteristics associated with tropical cyclone development in the North Indian Ocean during FGGE. *Mon. Weather Rev.*, *117*(2), 407-426.

Lee, C.S., (1989a), Observational analysis of tropical cyclogenesis in the western North Pacific. Part I: Structural evolution of cloud clusters. *J. Atmos. Sci.*, *46*(16), 2580-2598.

Lee, C.S. (1989b), Observational analysis of tropical cyclogenesis in the western North Pacific. Part II: Budget analysis. *J. Atmos. Sci.*, *46*(16), 2599-2616.

Li, T., 2006. Origin of the summertime synoptic-scale wave train in the western North Pacific. *J. Atmos. Sci.*, *63(3)*, 1093-1102.

Li, T. and B. Fu (2006), Tropical cyclogenesis associated with Rossby wave energy dispersion of a preexisting typhoon. Part I: Satellite data analyses. *J. Atmos. Sci.*, *63*(5), 1377-1389.

Li, T., X. Ge, B. Wang and Y. Zhu (2006), Tropical cyclogenesis associated with Rossby wave energy dispersion of a preexisting typhoon. Part II: Numerical simulations. *J. Atmos. Sci.*, *63*(5), 1390-1409.

Liu, K.S., and J.C. Chan (2012), Interannual variation of Southern Hemisphere tropical cyclone activity and seasonal forecast of tropical cyclone number in the Australian region. *Int. J. Climatol.*, *32*(2), 190-202.

McBride, J.L., and R. Zehr (1981), Observational analysis of tropical cyclone formation. Part II: Comparison of non-developing versus developing systems. *J. Atmos. Sci.*, *38*(6), 1132-1151.

Montgomery, M.T., M.E. Nicholls, T.A. Cram, and A.B. Saunders (2006b), A vortical hot tower route to tropical cyclogenesis. *J. Atmos. Sci.*, *63*(1), 355-386.

Montgomery, M.T. and R.K., Smith, 2010. *Tropical-cyclone formation: Theory and idealized modelling*. Naval postgraduate school Monterey CA, Dept. Meteorol.

Montgomery, M.T., L.L., Lussier III, R.W. Moore, and Z. Wang (2010), The genesis of Typhoon Nuri as observed during the Tropical Cyclone Structure 2008 (TCS-08) field experiment–Part 1: The role of the easterly wave critical layer. *Atmos. Chem. Phys.*, *10*(20), 9879-9900.

Montgomery, M.T., and R.K. Smith (2012), The genesis of Typhoon Nuri as observed during the Tropical Cyclone Structure 2008 (TCS08) field experiment–Part 2: Observations of the convective environment. *Atmos. Chem. Phys.*, *12*(9), 4001-4009.

Nolan, D. S. (2007), What is the trigger for tropical cyclogenesis? *Aust. Meteorol. Mag.*, *56*, 241-266.

Peng, M.S., B. Fu, T. Li, and D.E. Stevens (2012), Developing versus nondeveloping disturbances for tropical cyclone formation. Part I: North Atlantic. *Mon. Weather Rev.*, *140*(4), 1047-1066.

Perrone, T.J., and P.R. Lowe (1986), A statistically derived prediction procedure for tropical storm formation. *Mon. Weather Rev.*, *114*(1), 165-177.

Powell, M.D. (1990), Boundary layer structure and dynamics in outer hurricane rainbands. Part II: Downdraft modification and mixed layer recovery. *Mon. Weather Rev.*, *118*(4), 918-938.

Ramsay, H.A., L.M. Leslie, P.J. Lamb, M.B. Richman, and M. Leplastrier (2008), Interannual variability of tropical cyclones in the Australian region: Role of large-scale environment. *J. Climate*, *21*(5), 1083-1103.

Rappin, E.D., D.S. Nolan, and K.A. Emanuel (2010), Thermodynamic control of tropical cyclogenesis in environments of radiative-convective equilibrium with shear. *Q. J. Roy. Meteorol. Soc.*, *136*(653), 1954-1971.

Raymond, D.J., C. López-Carrillo, and L.L. Cavazos (1998), Case-studies of developing east Pacific easterly waves. *Q. J. Roy. Meteorol. Soc.*, *124*(550), 2005-2034.

Raymond, D.J. and S.L. Sessions (2007), Evolution of convection during tropical cyclogenesis. *Geophys. Res. Lett.*, *34*(6).

Raymond, D.J. and C. López Carrillo, (2011), The vorticity budget of developing typhoon Nuri (2008). *Atmos. Chem. Phys.*, *11*(1), 147-163.

Riemer, M., M.T. Montgomery, and M.E. Nicholls (2010), A new paradigm for intensity modification of tropical cyclones: thermodynamic impact of vertical wind shear on the inflow layer. *Atmos. Chem. Phys.*, *10*(7).

Riemer, M., and M.T. Montgomery (2011), Simple kinematic models for the environmental interaction of tropical cyclones in vertical wind shear. *Atmos. Chem. Phys.*, *11*(17), p.9395-9414.

Ritchie, E.A. and G.J. Holland (1999), Large-scale patterns associated with tropical cyclogenesis in the western Pacific. *Mon. Weather Rev.*, *127*(9), 2027-2043.

Ritchie, E.A. and W.M. Frank (2007), Interactions between simulated tropical cyclones and an environment with a variable Coriolis parameter. *Mon. Weather Rev.*, *135*(5), 1889-1905.

Rozoff, C.M., W.H. Schubert, B.D. McNoldy and J.P. Kossin (2006), Rapid filamentation zones in intense tropical cyclones. *J. Atmos. Sci.*, *63*(1), 325-340.

Rutherford, B., T.J. Dunkerton, and M.T. Montgomery (2015), Lagrangian vortices in developing tropical cyclones. *Q. J. Roy. Meteorol. Soc.*, *141*(693), 3344-3354.

Rutherford, B., M.A. Boothe, T.J. Dunkerton, and M.T. Montgomery (2018), Dynamical properties of developing tropical cyclones using Lagrangian flow topology. *Q. J. Roy. Meteorol. Soc.*, *144*(710), 218-230.

Sears, J. and C.S. Velden (2014), Investigating the role of the upper-levels in tropical cyclone genesis. *Tropical Cyclone Res. & Rev.*, *3*(2), 91-110.

Shu, S., F. Zhang, J. Ming, and Y. Wang (2014), Environmental influences on the intensity changes of tropical cyclones over the western North Pacific. *Atmos. Chem. Phys.*, *14*(12), 6329-6342.

Smith, R.K. and M.T. Montgomery (2012), Observations of the convective environment in developing and non-developing tropical disturbances. *Q. J. Roy. Meteorol. Soc.*, *138*(668), 1481-1739.

Tang, B. and K. Emanuel (2010), Midlevel ventilation's constraint on tropical cyclone intensity. *J. Atmos. Sci.*, *67*(6), 1817-1830.

Thorncroft, C. D., and K. Hodges, (2001), African easterly wave variability and its relationship to Atlantic tropical cyclone activity. *J Climate, 14*, 1166–1179.

Tippett, M.K., S.J. Camargo and A.H. Sobel (2011), A Poisson regression index for tropical cyclone genesis and the role of large-scale vorticity in genesis. *J Climate*, *24*(9), 2335-2357.

Tory, K.J., M.T. Montgomery, and N.E. Davidson (2006a), Prediction and diagnosis of tropical cyclone formation in an NWP system. Part I: The critical role of vortex enhancement in deep convection. *J. Atmos. Sci.*, *63*(12), 3077-3090.

Tory, K.J., M.T. Montgomery, N.E. Davidson, and J.D. Kepert (2006b), Prediction and diagnosis of tropical cyclone formation in an NWP system. Part II: A diagnosis of Tropical Cyclone Chris formation. *J. Atmos. Sci.*, *63*(12), 3091-3113.

Tory, K.J., N.E. Davidson, and M.T. Montgomery (2007), Prediction and diagnosis of tropical cyclone formation in an NWP system. Part III: Diagnosis of developing and nondeveloping storms. *J. Atmos. Sci.*, *64*(9), 3195-3213.

Tory K.J., and W.M. Frank (2010) Tropical cyclone formation. Chapter 2: Global perspectives on tropical cyclones. In: Chan J, Kepert JD (eds) World Scientific, Second Edition

Tory, K.J., R.A. Dare, N.E. Davidson, J.L. McBride, and S.S. Chand (2013a), The importance of low-deformation vorticity in tropical cyclone formation. *Atmos. Chem. Phys.*, *13*(4), 2115-2132.

Tory, K.J., S.S. Chand, R.A. Dare, and J.L. McBride (2013b), The development and assessment of a model-, grid-, and basin-independent tropical cyclone detection scheme. *J. Climate*, *26*(15), 5493-5507.

Tory, K.J., S.S. Chand, J.L. McBride, H. Ye, and R.A. Dare (2013d), Projected changes in late-twenty-first-century tropical cyclone frequency in 13 coupled climate models from phase 5 of the Coupled Model Intercomparison Project. *J. Climate*, *26*(24), 9946-9959.

Tory, K.J., H. Ye, and R.A. Dare (2018), Understanding the geographic distribution of tropical cyclone formation for applications in climate models. *Climate Dynam.*, *50*(7-8), 2489-2512.

Tuleya, R.E. and Y. Kurihara (1981), A numerical study on the effects of environmental flow on tropical storm genesis. *Mon. Weather Rev.*, *109*(12), 2487-2506.

Tuleya, R.E. and Y. Kurihara (1982), A note on the sea surface temperature sensitivity of a numerical model of tropical storm genesis. *Mon. Weather Rev.*, *110*(12), 2063-2069.

Tuleya, R.E., (1991), Sensitivity studies of tropical storm genesis using a numerical model. *Mon. Weather Rev.*, *119*(3), 481-733.

Wang, C.C. and G. Magnusdottir (2005), ITCZ breakdown in three-dimensional flows. *J. Atmos. Sci.*, *62*(5), 1497-1512.

Wang, C.C. and G. Magnusdottir (2006), The ITCZ in the central and eastern Pacific on synoptic time scales. *Mon. Weather Rev.*, *134*(5), 1405-1421.

Wang, Z., M.T. Montgomery, and T.J. Dunkerton (2010a), Genesis of pre–Hurricane Felix (2007). Part I: The role of the easterly wave critical layer. *J. Atmos. Sci.*, *67*(6), 1711-1489.

Wang, Z., M.T. Montgomery, and T.J. Dunkerton (2010b), Genesis of pre–Hurricane Felix (2007). Part II: Warm core formation, precipitation evolution, and predictability. *J. Atmos. Sci.*, *67*(6), 1730-1744.

Wang, Z., M.T. Montgomery, and C. Fritz (2012), A first look at the structure of the wave pouch during the 2009 PREDICT–GRIP dry runs over the Atlantic. *Mon. Weather Rev.*, *140*(4), 1144-1163.

Wang, Z. (2012), Thermodynamic aspects of tropical cyclone formation. *J. Atmos. Sci.*, *69*(8), 2433-2451.

Wang, Z. (2014), Role of cumulus congestus in tropical cyclone formation in a high-resolution numerical model simulation. *J. Atmos. Sci.*, *71*(5), 1681-1700.

Xu, Y., Li, T. and M. Peng (2013), Tropical cyclogenesis in the western North Pacific as revealed by the 2008–09 YOTC data. *Weather Forecast.*, *28*(4), 1038-1056.

Zehr, R. (1992), Tropical cyclogenesis in the western North Pacific. NOAA Tech. Rep. 61, 181pp.

Zeng, Z., Y. Wang, and L. Chen (2010), A statistical analysis of vertical shear effect on tropical cyclone intensity change in the North Atlantic. *Geophys. Res. Lett.*, *37*(2).

Zhang, D.L., and L. Zhu (2012), Roles of upper-level processes in tropical cyclogenesis. *Geophys. Res. Lett.*, *39*(17).

Zhao, H. and G.B. Raga (2015), On the distinct interannual variability of tropical cyclone activity over the eastern North Pacific. *Atmósfera*, *28*, 161-178.

Zong, H. and L. Wu (2015), Re-examination of tropical cyclone formation in monsoon troughs over the western North Pacific. *Adv. Atmos. Sci.*, *32*(7), 924-934.

Table 1. The order of importance of variables in each ocean basin based on the statistically significant values at the 95% significance level of the BDI index at Day-2 and Day0 (the day of TD declaration).

BASIN	Order of variables (Day-2)	Order of variables (Day0)
NA-MDR	TCW, MPI, Omega, RVor	RVor, TCW, Ushear,Omega
ENP	TCW, Ushear, RVor, Omega	TCW, Ushear, Omega, Beta*
WNP	RVor, Omega, MPI, TCW	RVor, Omega, MPI,TCW
WNP-P	RVor, TCW, Ushear, MPI	RVor, TCW, Omega, MPI
NI	--	Omega
SI	TCW, Omega	TCW, Omega, RVor, MPI
SP	Ushear, MPI,TCW, RVor, Beta*	Ushear, MPI,TCW, RVor, Omega
AUS	RVor, TCW, Ushear	RVor, TCW, Ushear, Omega, MPI

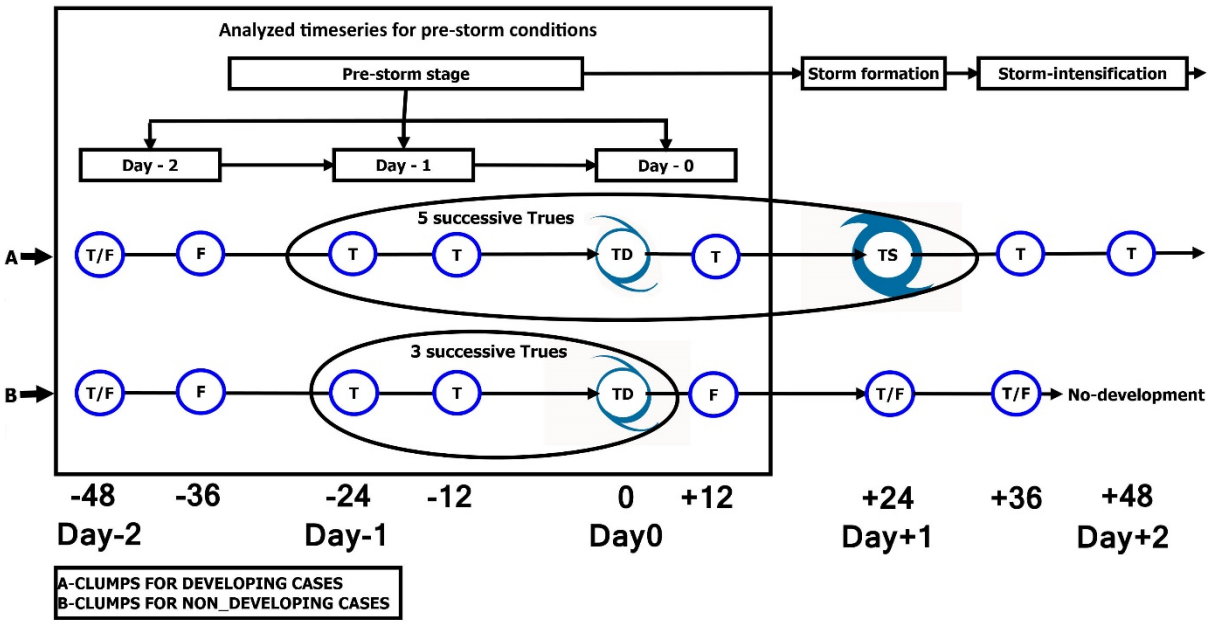

Figure 1. Diagram showing the tracks of developing and non-developing tropical depressions with F(False) indicating that the core thresholds are not satisfied and T(True) where the thresholds are satisfied. The 3rd consecutive true is the TD declaration time for both developing and non-developing TDs. Path A shows that all TSs were once TDs, and path B is a TD that did not develop into TS.

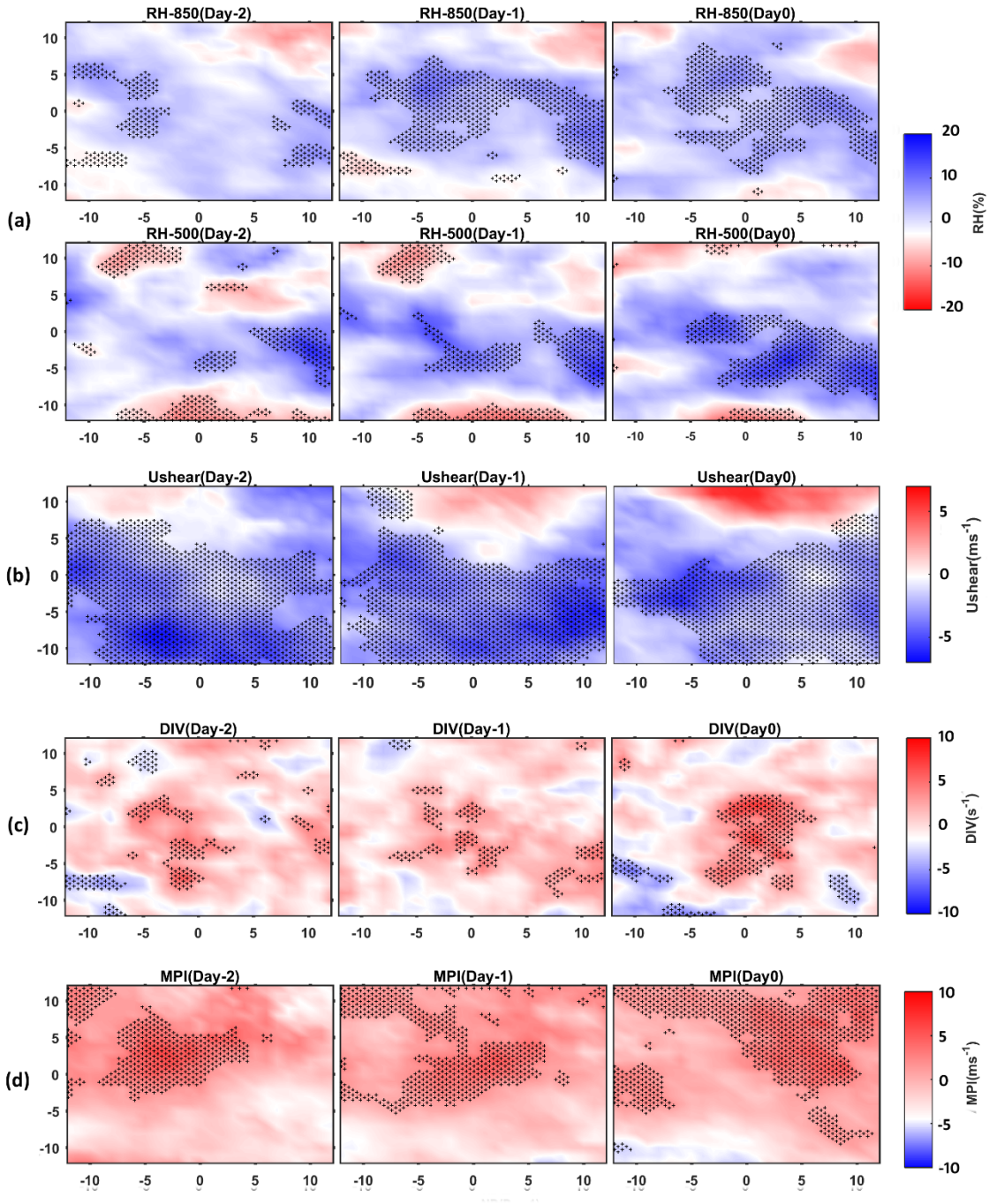

Figure 2. Differences in spatial composites of developing and non-developing cases (DV minus ND) within the 24° × 24° *box region region around the circulation center over the*

North Atlantic basin, (a) 850 and 500 hPa RH, (b) Ushear, (c) DIV and (d) MPI. The stippling indicates the 95% significance level differences.

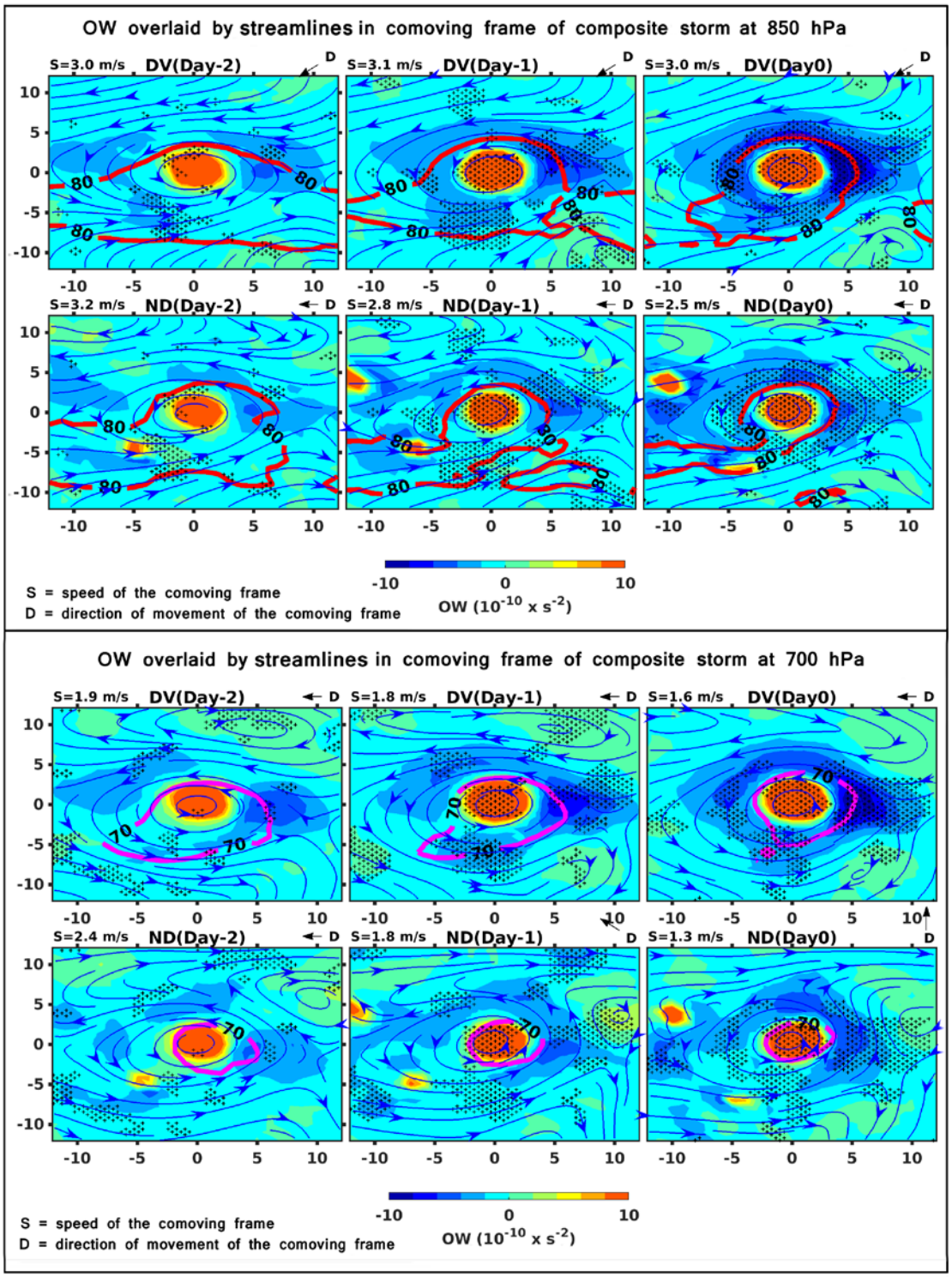

Figure 3. OW overlaid by streamlines computed in a co-moving frame for DV and ND cases at 850 and 700hPa over the North Atlantic basin. The x and y-axis indicating the distance from the center in degrees, the red and magenta contours indicate 80% and 70% RH, respectively and stippling indicates the 95% significance level differences between DV and ND cases.

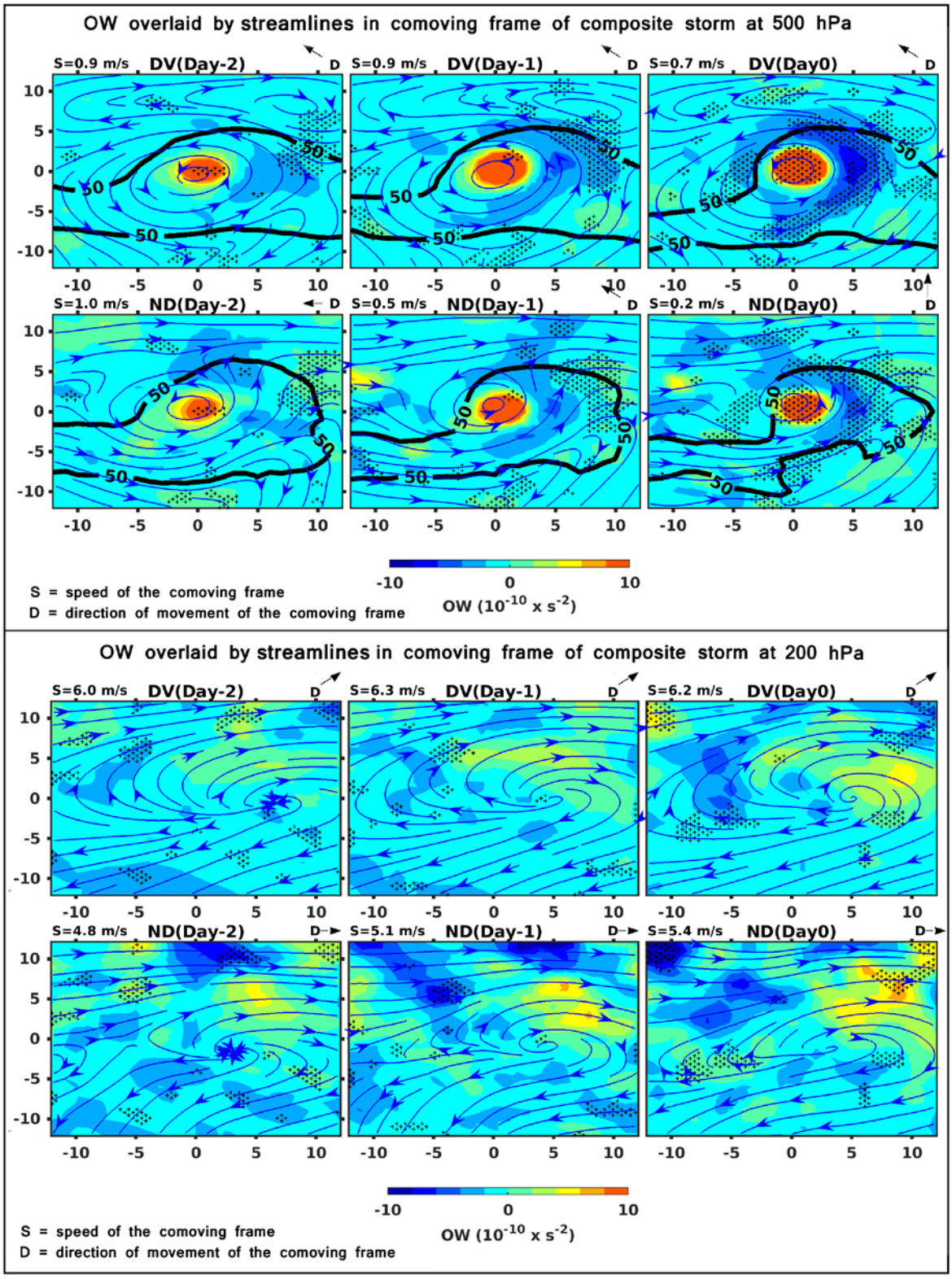

Figure 4. The same as Figure 3 over the 500 and 200 hPa, the black contour indicate the 50% RH.

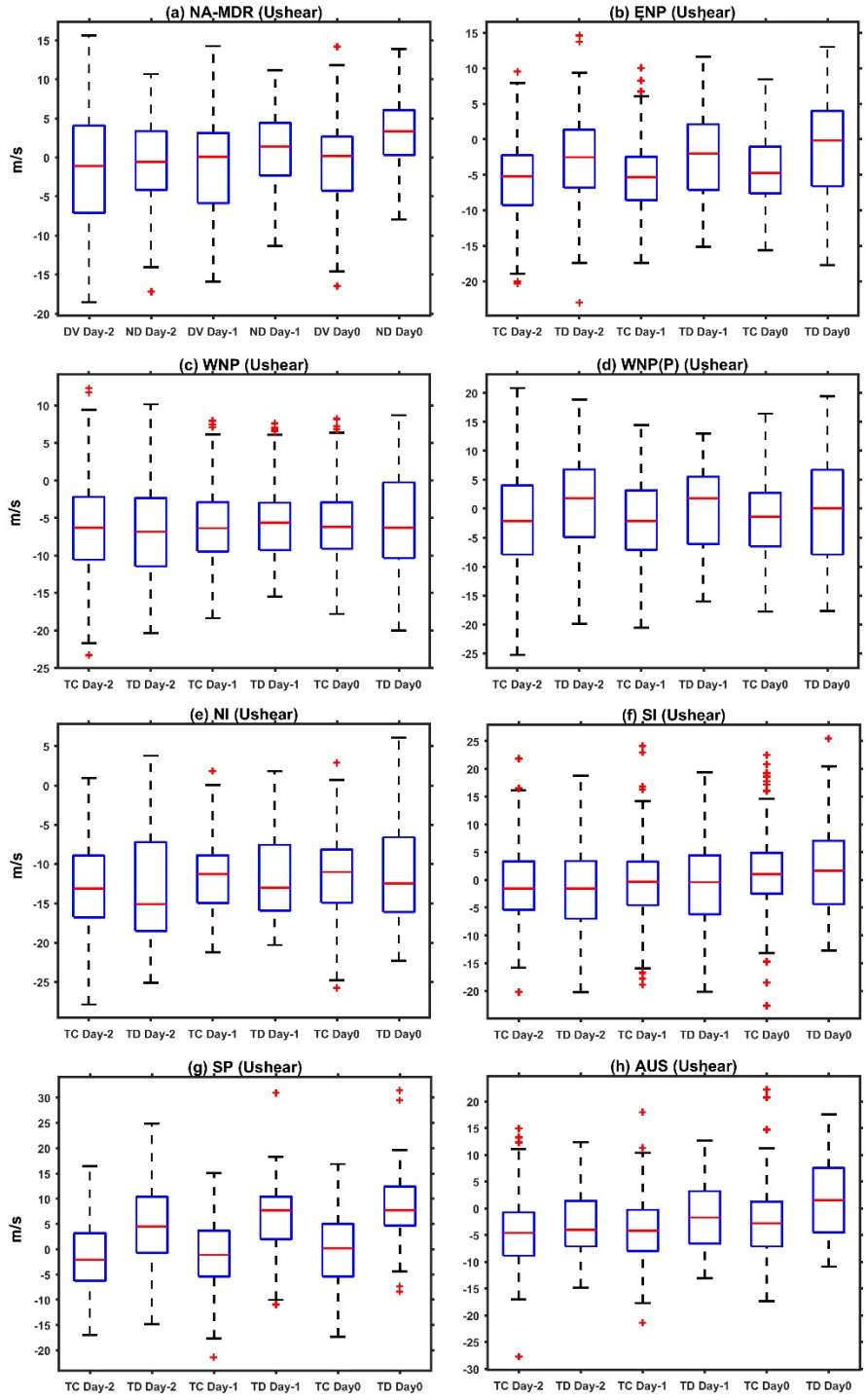

Figure 5. Box-plots of averaged Ushear for DV and ND cases within a 12°×12° box region. The horizontal line of the box indicates median of the distribution, the left, and right box

edges show 75th and 25th percentiles, the whiskers indicate maximum and minimum values and the red crosses indicate outliers. The statistical significance of Ushear is given in Figure 6.

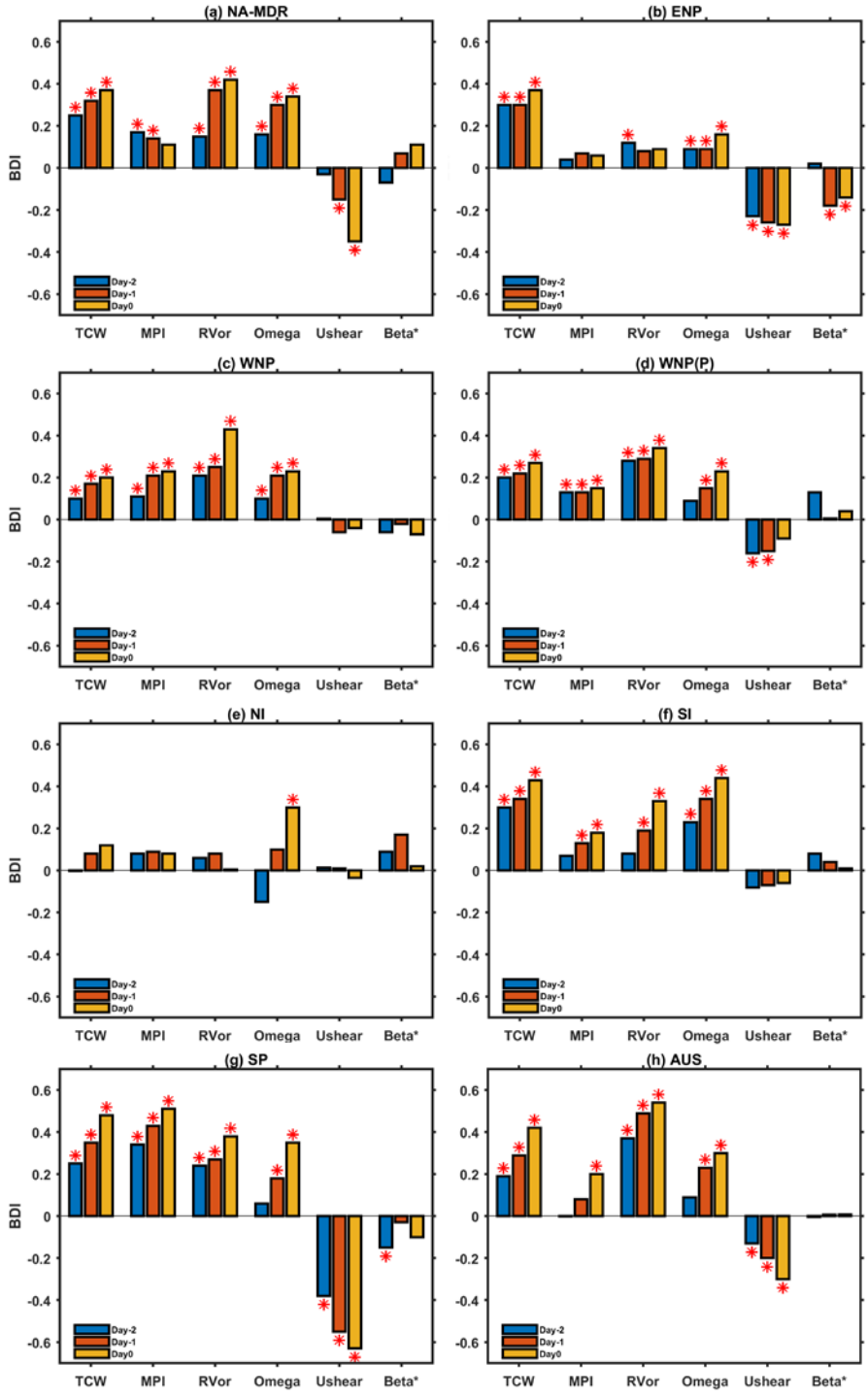

Figure 6. Basinwide BDI index of environmental variables for PDV48 and PND48 cases on Day-2, Day-1, and Day0. Positive values of the BDI index for TCW, MPI, RVor, and Omega

indicate more favorable conditions for development, while negative values of Ushear, Beta are more favorable (* indicates a 95% significance level). For parameterwise comparison of the BDI values refer to the Figure S14.*

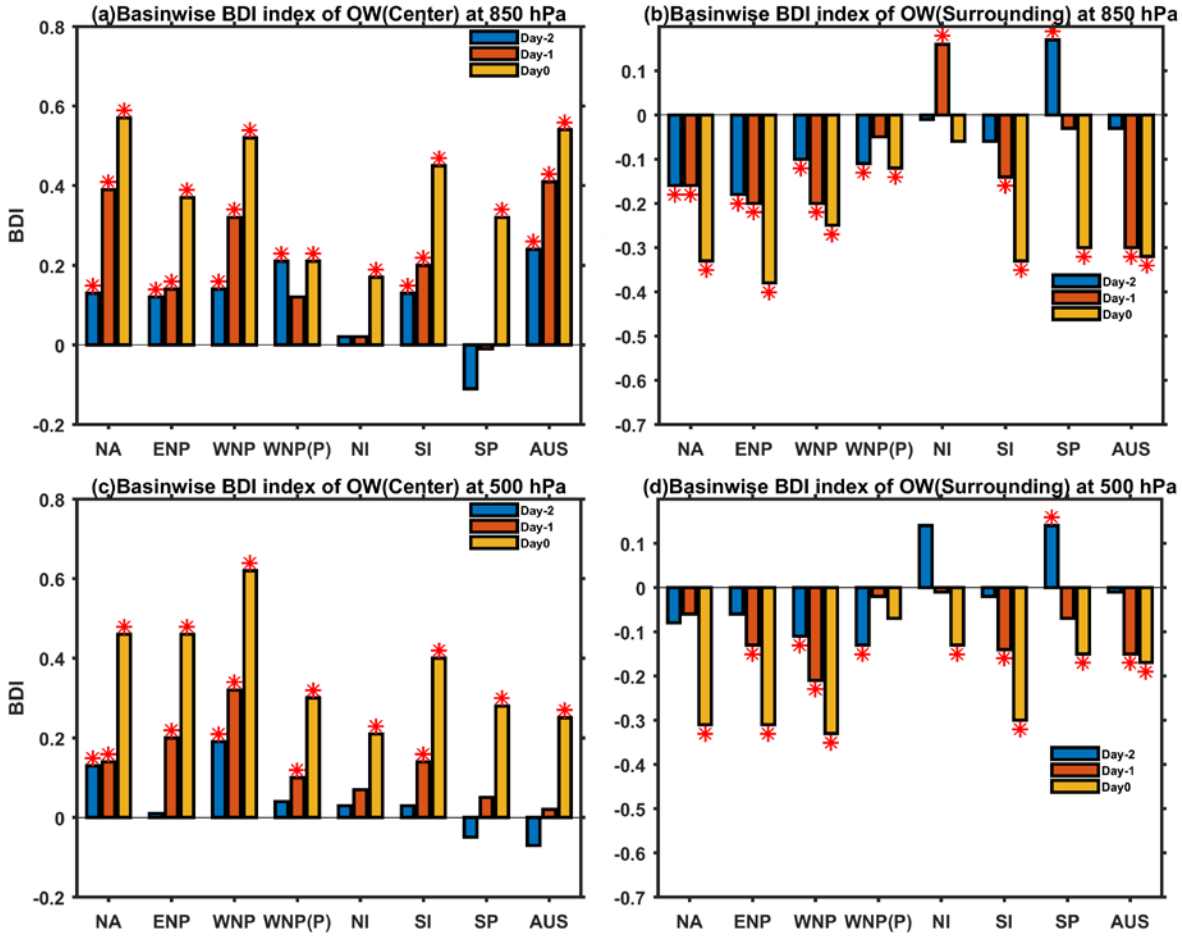

Figure 7. Basinwide BDI index of OW center and OW surrounding for DV and ND cases at 850 and 500 hPa levels on Day-2, Day-1, and Day0. Positive values of OW center variable and negative values of OW surrounding variable are more favorable for TS formation (indicates a 95% significance level).*

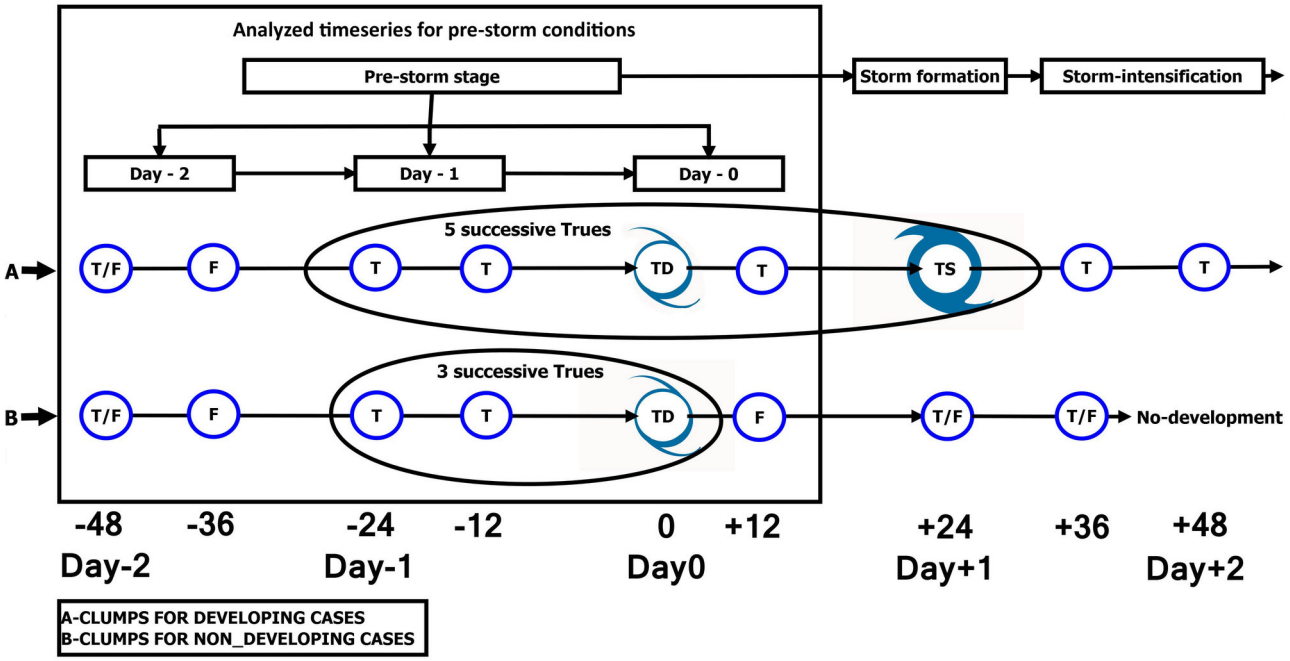

2019JD032006-f01-z-.jpg

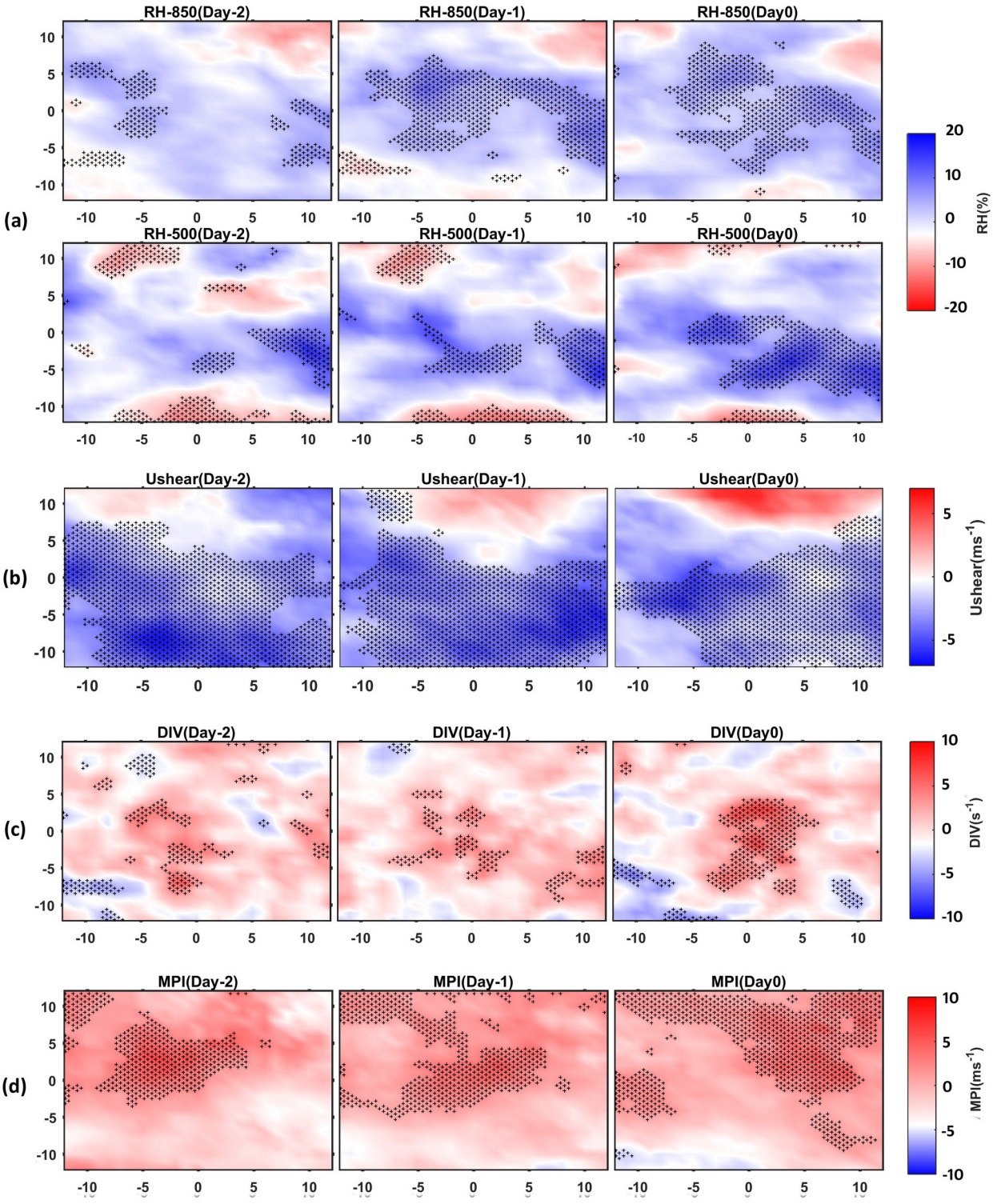

2019JD032006-f02-z-.jpg

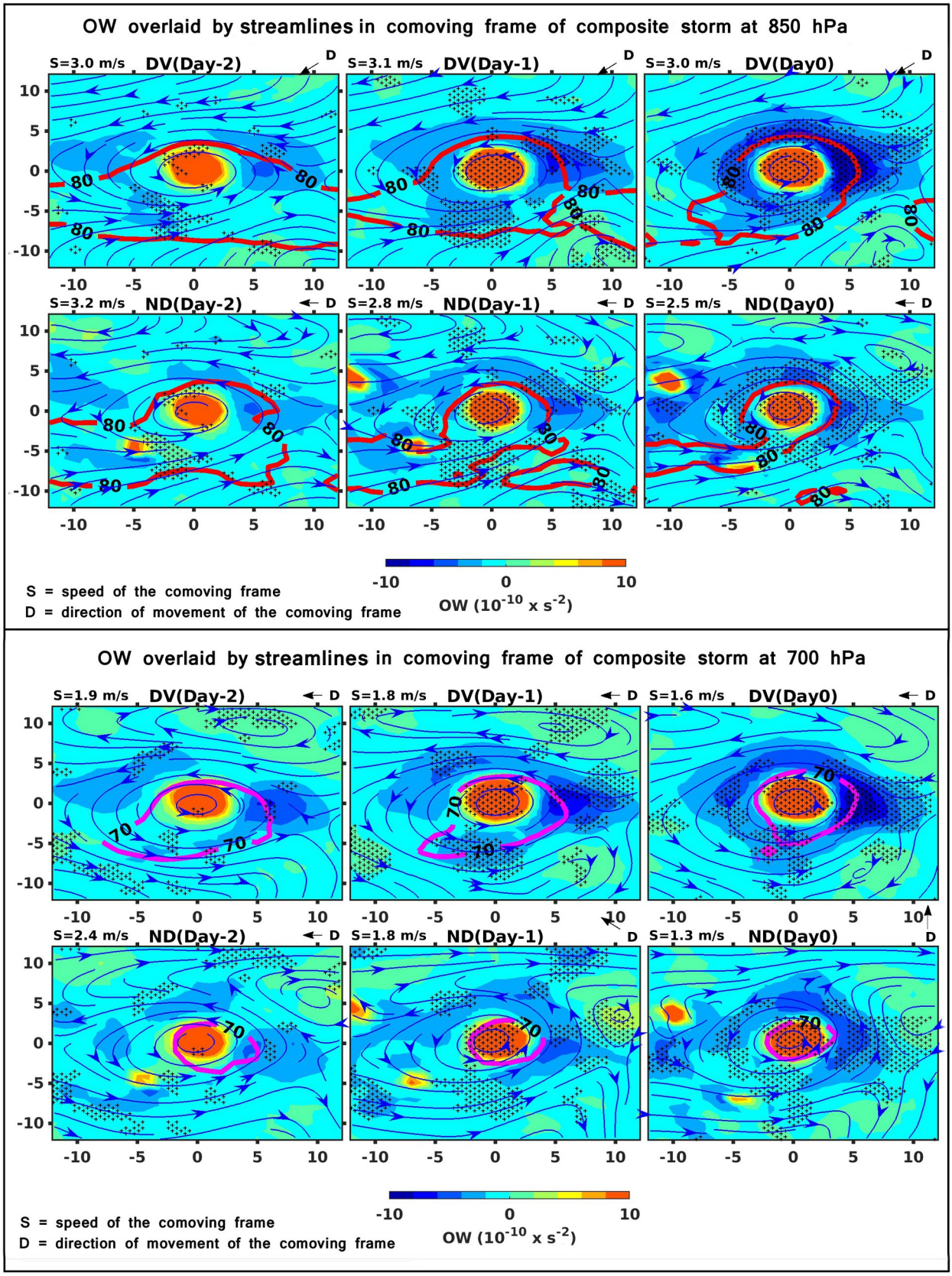

2019JD032006-f03-z-.jpg

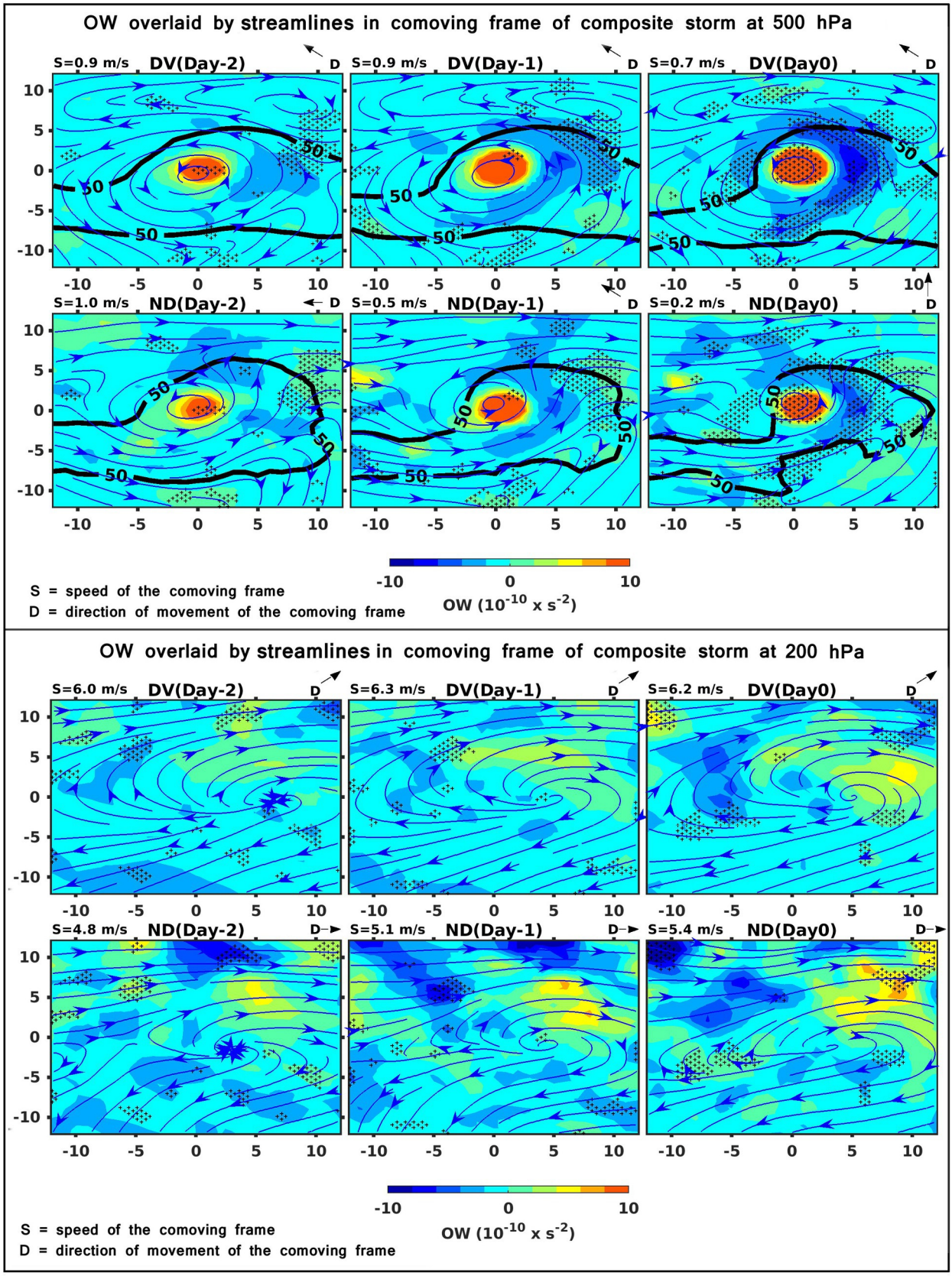

2019JD032006-f04-z-.jpg

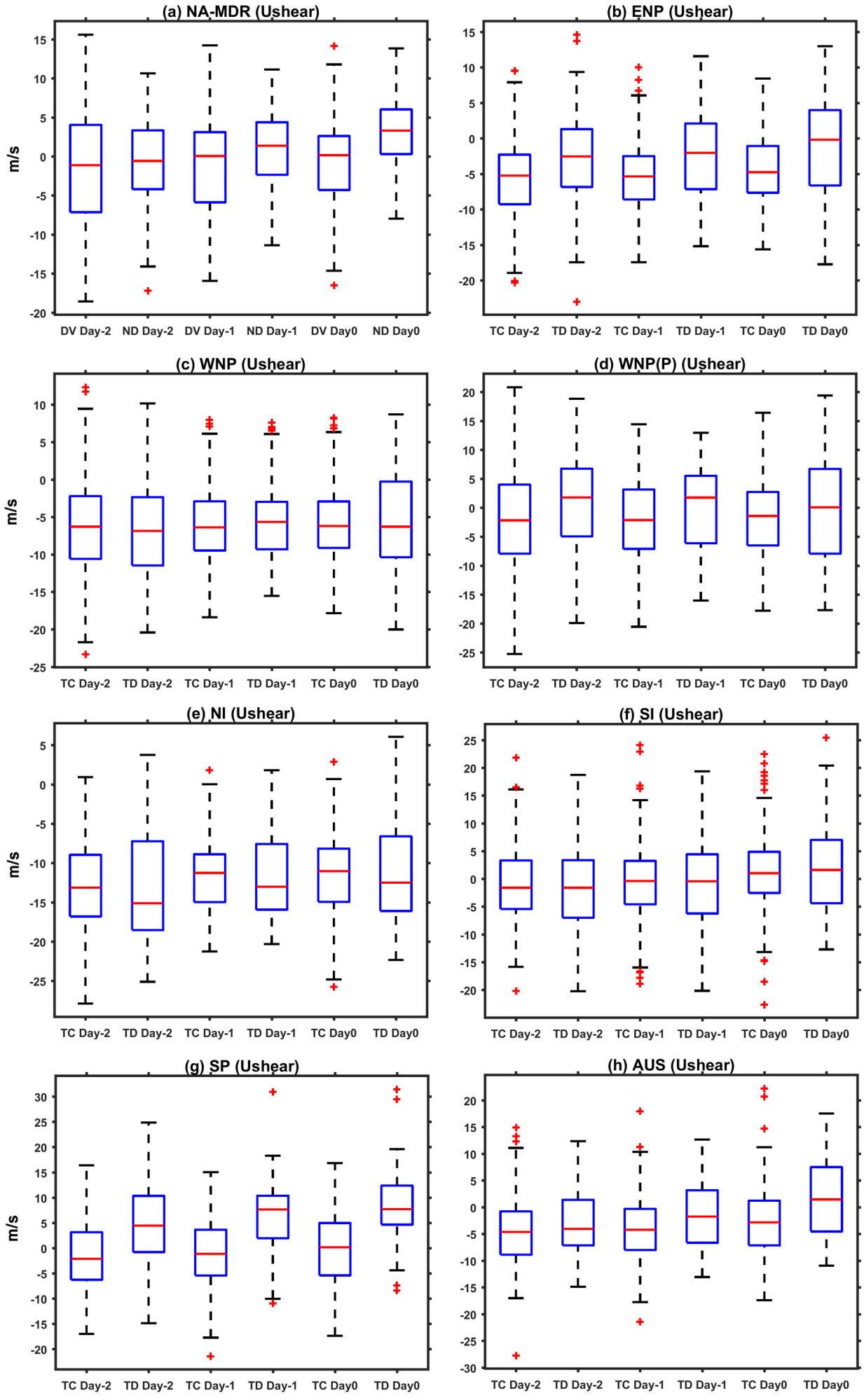

2019JD032006-f05-z-jpg

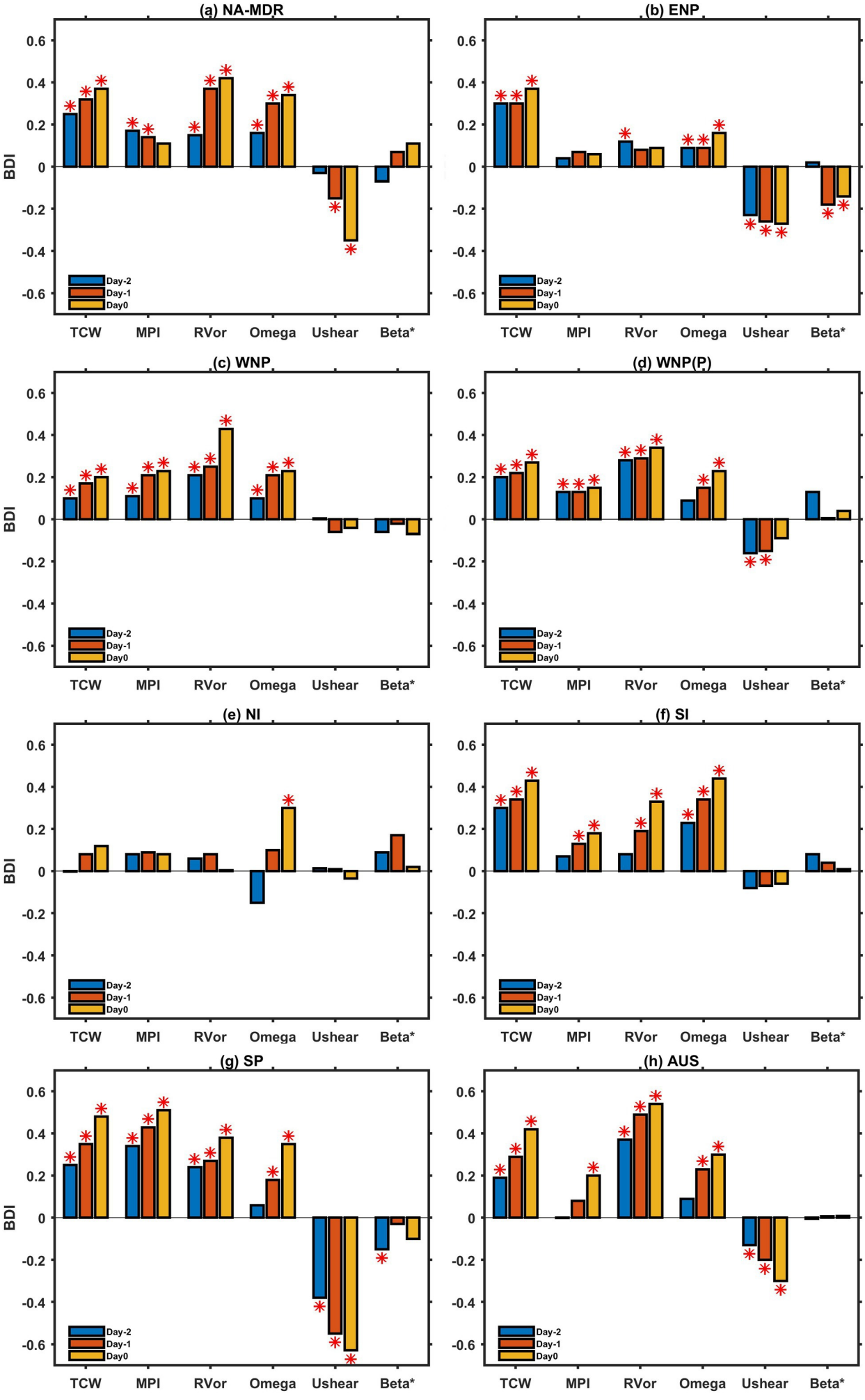

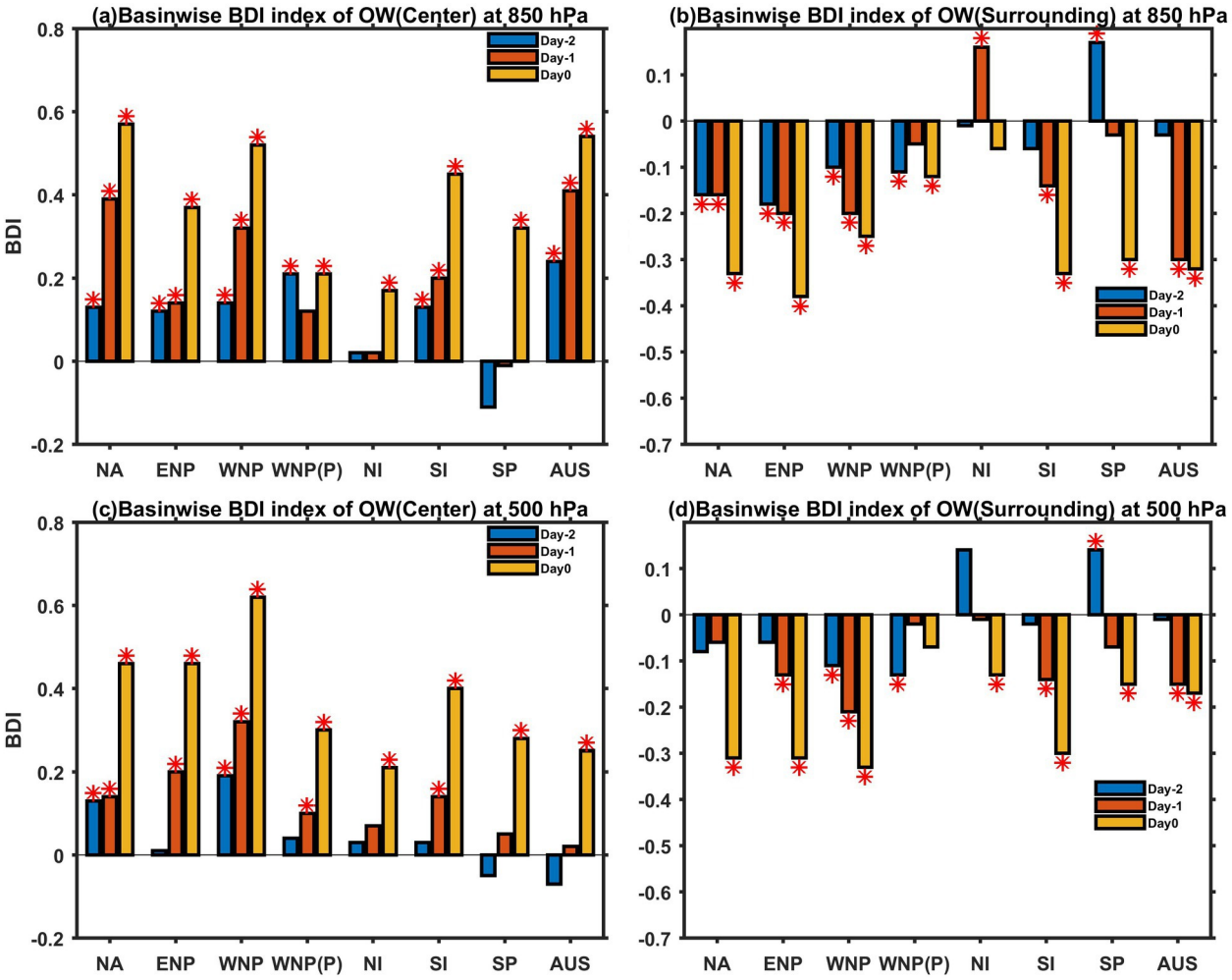

2019JD032006-f07-z-.jpg